







Review Article

Spontaneous U(1) Symmetry **Breaking and Phase Transitions** in Rotating Interacting Bose Gases

Sun Wenming*

Graduate School of Science, University of Tokyo, 113-8654, Japan

Received: 14 November, 2025 Accepted: 20 November, 2025 Published: 24 November, 2025

*Corresponding author: Sun Wenming, Graduate School of Science, University of Tokyo, 113-8654, Japan, E-mail: ywtbsygk@pgu.edu.pl

Keywords: U(1) symmetry breaking; Rotating Bose gas: Phase transition

Copyright License: © 2025 Wenming S. This is an open-access article distributed under the terms of the Creative Commons Attribution License, which permits unrestricted use, distribution, and reproduction in any

medium, provided the original author and source are

https://www.mathematicsgroup.us



Abstract

We investigate spontaneous U(1) symmetry breaking and the associated phase transitions in rotating interacting Bose gases. Using a theoretical framework that combines mean-field analysis with rotational dynamics, we analyze how rigid rotation modifies the condensate structure, critical behavior, and low-energy excitation spectrum. We identify the emergence of Goldstone modes (massless rotons and massive phonons) in the symmetry-broken phase and clarify their role in mediating lowenergy excitations—findings that remain robust at low momentum regardless of rotation. A key result is the angular velocity (Ω) dependence of the critical temperature (Tc) for U(1) phase transition, where Tc scales as $\Omega^{(1/3)}$, distinct from the $\Omega^{(2/5)}$ (nonrelativistic) and $\Omega^{(1/4)}$ (ultrarelativistic) scaling observed in noninteracting rotating Bose gases. Rotation also alters the temperature dependence of the thermodynamic potential minima, changing the characteristic factor from (1 - t) (t = T/Tc for nonrotating systems) to (1 - t³) for rotating gases. We further demonstrate that rotation preserves the second-order nature of the phase transition, while modifying the critical exponents and reducing the discontinuity in heat capacity with increasing Ω . Additionally, we define a σ meson dissociation temperature (Tdiss) characterized by mσ(Tdiss) = 2mπ(Tdiss), showing that Tdiss is always lower than Tc. Thermal mass corrections are shown to ensure the validity of Goldstone's theorem in the rotating frame, even in the chiral limit. These results deepen our understanding of the interplay between symmetry, rotation, and many-body interactions, with implications for interpreting extreme conditions in heavy-ion collisions and compact astrophysical objects, while advancing the theoretical framework for phase structures in rotating Bose systems.

PACS: 05.30.Jp;11.30.Qc;67.85.-d;64.60.-i

I. Introduction

One of the primary goals of modern Heavy Ion Collision (HIC) experiments is to study matter under extreme conditions and its transitions through various phases. In Quantum Chromodynamics (QCD), these phases range from the deconfined quark-gluon plasma to the confined hadron phase, which consists of mesons and baryons. Mesons, as composite particles made up of a quark and an antiquark, are often regarded as (pseudo-)Goldstone bosons arising from the spontaneous breaking of chiral symmetry. Key questions related to the phase transition of matter created in HIC experiments focus in particular on the order of the phase transition and the location of the critical endpoint [1-5]. Answers to these questions provide valuable insights into astrophysical and cosmo-logical models of the early universe [6,7]. Both of these properties are affected by external conditions, such as ex-ternal electromagnetic fields and rotation. Intense mag- netic fields are believed to be generated in the early stages of noncentral HICs. Depending on the initial conditions, the strength of the magnetic fields is estimated to be ap-proximately B ~ 1018 - 1020 Gauß in the early stages after these collisions [8,9]. In recent years, several stud- ies have explored the QCD phase diagram in the presence of magnetic fields. Novel effects, such as magnetic and inverse magnetic catalysis are associated with the effect of constant background magnetic fields on the nature of the chiral phase transition and the location of the critical point [10-12]. Recently, several studies have investigated the effect of rotation on quark matter created

in HIC experiments. This matter is believed to experience ex-tremely high vorticity, with an angular velocity reaching up to 1022 Hz [13,14]. Extensive research has focused on how rotation influences the thermodynamic properties of relativistic fermionic systems [15-20]. One notable example is the chiral vortical effect, which is related to the transport properties of the quark matter produced after HICs and provides insights into the topological aspects of QCD [21]. When examining the thermodynamic properties of rotating Fermi gases using field theoretical meth- ods, it is advantageous to assume rigid rotation with a constant angular velocity [22,23]. The impact of rigid rotation on QCD phase transitions, including chiral and confinement/ deconfinement, has been studied with and without boundary conditions, e.g., in [15,24]. In [24], it is shown that at finite temperature the phase diagram of a uniformly rotating system exhibits, in addition to a confining and a deconfining phase at low and high tem-peratures, a mixed inhomogeneous phase at intermediate temperatures.

Several studies have also explored both relativistic bosons [25-35] and the linear sigma model with quarks [36-39] under rigid rotation. In [26], a spin-one gluon gas under rigid rotation is analyzed, revealing that at temperatures below a certain supervortical temperature, the moment of inertia of a rotating spin-one gluon plasma becomes negative. This phenomenon indicates a thermodynamic instability and is associated with the negative Barnett effect, where the total angular moment of the system opposes the direction of its angular velocity. For spin-zero bosons in the presence of imaginary rotation, ninionic statistics arise, modifying the standard Bose-Einstein distribution with a statistical angle. Under specific conditions, these bosons exhibit fermionic-like behavior and display fractal thermodynamics that depend on the angle of imaginary rotation [27]. A separate study in [28] investigated the thermodynamics of spin-zero com- plex scalar fields under rigid rotation, revealing that ther-modynamic instabilities emerge at high temperatures and large coupling constants. These instabilities include neg- ative moment of inertia and heat capacity. Finally, in [30], the Bose-Einstein (BE) condensation of a free Bose gas subjected to rigid rotation is investigated in both rel- ativistic and nonrelativistic limits. It is demonstrated that rotation not only modifies the equation of state of the system but also impacts the transition temperature for BEC and the fraction of condensates. Specifically, it is shown that the critical temperature of a rotating Bose gas is lower than that of a nonrotating gas; however, as the angular velocity increases, the critical temperature of the rotating gas also rises. Additionally, an analysis of the heat capacity of a nonrelativistic rotating free Bose gas indicates that rotation alters the nature of the BEC phase transition from continuous to discontinuous. The present paper aims

to extend these findings to an inter- acting Bose gas under rigid rotation.

We begin with the Lagrangian density of a complex Klein-Gordon field ϕ that includes a self-interaction term $\lambda(\phi \star \phi)$ 2 with a coupling constant λ . To introduce rigid rotation we use a metric including the angular velocity Ω . In the first part of this paper, we introduce a chem-ical potential μ corresponding to the global U(1) sym- metry of the Lagrangian. For later analysis, we expand the Lagrangian density around a classical configuration $|\langle \phi |$ ≡ v. Following standard methods [40,41] and utiliz- ing an appropriate Bessel-Fourier transformation [29,30], we derive the free propagator of this model. This propa- gator is subsequently employed to compute the thermo-dynamic potential as a function of μ , Ω , and the energy dispersion relation ϵ^{\pm} k. As it turnss out, the spontaneous breaking of U(1) symmetry occurs for m < μ . In this regime, we find two distinct energy branches; one corre-sponding to a massive phonon and the other to a massless roton. It is noteworthy that the rotation does not alter ϵk at low momentum, and the results are similar to the nonrotating case [42].

In the second part of this paper, we explore the im-pact of rotation on the spontaneous breaking of U(1) symmetry, focusing specifically on the case of zero chem-ical potential. Our primary emphasis is on the T and Ω dependence of the critical temperature of the corre-sponding phase transition, as well as two masses m₁ and m₂, which are identified with the masses of the σ and π mesons, respectively. We begin by considering the ther- modynamic potential discussed in the first part of this paper. Apart from a classical part, it consists of a ther- mal and a vacuum contributions. By employing a novel method for summing over the quantum number ℓ related to rotation, we perform a hightemperature expansion. Combining the classical and the thermal parts, we de-rive an analytical expression for the critical temperature of U(1) phase transition Tc, which is found to be pro- portional to $\Omega^{1/3}$.

Furthermore, we show that the min- ima of this potential are proportional to $(1 - t^3)$, where $t \equiv T/T$ is the reduced temperature. This contrasts with the behavior observed in a nonrotating Bose gas, where the minima are

described by the factor $\binom{1-t_0^2}{2}$ with $t_0 \equiv T/Tc^{(0)}$. (Here, suband superscripts zero correspond to nonrotating Bose gas.) We also demonstrate that when sub-stituting these minima into m₁ and m₂, they become imaginary in the symmetryrestored phase, analogous to the behavior in a nonrotating Bose gas. This issue is addressed by adding the thermal masses that arise from one-loop perturbative contributions to m₁ and m₂. By following this method, we confirm that the Goldstone theorem is satisfied in the symmetry-restored phase.

We then compute the vacuum part of the potential by adding the appropriate counterterms and performing dimensional regularization. Our findings extend the results from [43], where the vacuum contribution to the effective action for a $\lambda \phi^4$ theory was computed. We add this potential to the classical and thermal parts of the potential, minimize the resulting expression, and exam- ine how the minima depend on temperature T for fixed angular velocity Ω . We show that, similar to the behav- ior observed in a noninteracting Bose gas [30], rotation reduces the critical temperature of the phase transition, which then increases as Ω rises. Additionally, by plug-ging these minima into the corresponding expressions to m₁ and m₂ (or equivalently m σ and m_{_}), we investigate the T dependence of σ and π meson masses for fixed Ω . As expected, in the symmetryrestored phase, we find $m_{\sigma} = m\pi$. This equality indicates that at T_c the min- ima of the corresponding potential vanish, suggesting a second-order phase transition, even in the presence of rigid rotation.

Finally, we focus on the nonperturbative ring contribution to the potential described above. We present a full derivation of the ring potential in the presence of rotation. Based on the findings in [43], we expect that the addition of the ring potential will alter the order of the phase transition. Our results indicate that when rotation is absent $(\Omega = 0)$, a discontinuous phase transition occurs at a specific temperature. In contrast, when rotation is present ($\Omega \neq 0$), the phase transition remains continuous. Furthermore, we define a σ disso- ciation temperature, denoted by Tdiss, which is charac-terized by m_{σ} (Tdiss) = $2m\pi$ (Tdiss) and show that Tdiss is less than the critical temperature.

The organization of this paper is as follows: In Sec. II, we introduce the rigid rotation in the Lagrangian density of a complex scalar field in the presence of a finite chemical potential. We derive the corresponding free propagator, determine the full thermodynamic potential of this model, and explore how rotation affects the spontaneous breaking of global U(1) symmetry. In Sec. III, we focus on the special case of μ = 0 and systematically deter- mine the full thermodynamic potential, which consists, apart from the classical part, of a thermal and a vacuum contribution. After examining the effect of rotation on the Goldstone theorem, we add the nonperturbative ring contribution to this potential, which is explicitly derived for the case of a rotating complex scalar field. In Sec. IV, the numerically solve the corresponding gap equation for the full potential with and without the ring potential. We investigate the T dependence of the corresponding min- ima for fixed Ω . Additionally, we determine the T and Ω dependence of m_{σ} and $m\pi$, along with the σ dissoci- ation temperatures. Section V concludes the paper with a compact summary of our findings. In Appendix A, we present the hightemperature expansion in the presence of a rigid rotation.

Notably, we apply a method intro-duced in [30] to sum over ℓ. Appendices B and C contain derivations of formulas (III.27) and (III.34), while the derivation of (III.44) is detailed in Appendix D.

From a broader physical perspective, this study bears important implications for understanding rotating quantum fluids—covering systems like the high-vorticity quark-gluon plasma in heavy-ion collisions and the superfluid cores of neutron stars (where interactions dominate quantum behavior). By clarifying how rotation regulates U(1) symmetry breaking, critical temperatures, and Goldstone mode dynamics in interacting Bose gases, we provide a theoretical framework to interpret experimental signatures of rotation-induced phase transitions (e.g., modified condensate fractions or excitation spectra in quantum gas experiments). Additionally, the Ω -dependent scaling of Tc $(\Omega^{(1/3)})$ and the preservation of secondorder phase transitions under rotation offer new insights for controlling quantum coherence in rotating systems relevant for quantum simulations of extreme astrophysical environments or the design of rotation-tunable BECbased devices. Ultimately, this work bridges fundamental field theory, condensed matter physics, and astrophysics, advancing our understanding of the collective behavior of strongly interacting quantum fluids.

II. Interacting charged scalars under rigid rotation

A. The free propagator

We start with the Lagrangian density of a charged scalar field φ

$$L = g^{uv} \partial^{u} \phi \star \partial^{v} \phi - m^{2} \phi \star \phi - \lambda (\phi \star \phi)^{2}$$
 (II.1)

with the metric

$$g_{\mu\nu} = \begin{pmatrix} 1 - r^2 \Omega^2 & y\Omega & -x\Omega & 0 \\ y\Omega & -1 & 0 & 0 \\ -x\Omega & 0 & -1 & 0 \\ 0 & 0 & 0 & -1 \end{pmatrix}$$
(II.2)

describing a rigid rotation. Here, m is the rest mass and 0 < λ < 1 is the coupling constant, describing the strength of the interaction. The spacetime coordinate is described by $x^{\mu} = (t, t)$ x, y, z) and $r^2 \equiv x^2 + y^2$. More-over, Ω is the constant angular velocity of a rigid rotation around the z-axis. The above Lagrangian is invariant un- der global U(1) transformation

$$\varphi(x) \to e^{-i\alpha} \varphi(x), \quad \varphi \star (x) \to e^{i\alpha} \varphi \star (x),$$
 (II.3)

with α a real constant phase. Plugging the metric into (II.1), we obtain

$$L = |(\partial_0 - i\mu - i\Omega L_z)\phi|^2 - |\nabla\phi|^2 - m^2|\phi|^2 - \lambda|\phi|^4$$
 (II.4)

where the chemical potential μ corresponding to the global U(1) symmetry (II.3) is introduced. The z-component of the angular momentum, L_x , is defined by $L_x = i(y\partial x - x\partial y)$. To investigate the spontaneous breaking of U(1) symmetry, we rewrite L in terms of real fields $\phi 1$ and $\phi 2$ appearing in

 $\phi = 1/\sqrt{(\phi 1 + i\phi 2)}$ and perform the shift $\phi_i \to \phi_i + \phi_i$ with $\Phi^2 = \begin{pmatrix} v \\ 0 \end{pmatrix}$ and v = const. We arrive at

$$\mathcal{L} = \sum_{i=0}^{4} \mathcal{L}_i, \tag{II.5}$$

with

$$\mathcal{L}_{0} = \frac{1}{2} \left(\mu^{2} - m^{2} \right) V^{2} - \frac{\lambda}{4} V^{4},$$

$$\mathcal{L}_{_{1}}=(\mu^{2}-m^{2})v\varphi_{_{1}}-\mu v\partial_{_{0}}\varphi_{_{2}}-\lambda v^{3}\varphi_{_{1}}+i\mu\Omega vL_{_{2}}\varphi_{_{2}}$$

$$\mathcal{L}_{2} = \frac{1}{2} \begin{cases} \left(\partial_{0}\varphi_{1}\right)^{2} + \left(\partial_{0}\varphi_{2}\right)^{2} - \left(\nabla\varphi_{1}\right)^{2} - \left(\nabla\varphi_{2}\right)^{2} \\ + \left(\mu^{2} - m^{2}\right)\left(\varphi_{1}^{2} + \varphi_{2}^{2}\right) + 2\mu\left(\varphi_{2}\partial_{0}\varphi_{1} - \varphi_{1}\partial_{0}\varphi_{2}\right) \\ -\lambda\left(3v^{2}\varphi_{1}^{2} + v^{2}\varphi_{2}^{2}\right) \end{cases}$$

$$\begin{split} &-\Omega^2\Big[(L_z\varphi_1)^2+(L_z\varphi_2)^2\Big]-2i\Omega\Big[(\partial_0\varphi_1+\mu\varphi_2)L_z\varphi_1\Big]\\ &-2i\Omega\Big[(\partial_0\varphi_2-\mu\varphi_1)L_z\varphi_2\Big] \end{split}$$

$$\mathcal{L}_{3} = -\lambda V \varphi_{1} \left(\varphi_{1}^{(2)} + \varphi_{2}^{(2)} \right)$$

$$\mathcal{L}_{4} = -\frac{\lambda}{4} \left(\varphi_{1}^{2} + \varphi_{2}^{2} \right)^{2} \tag{II.6}$$

The classical part of the Lagrangian, L₀, defines the classical (zero mode) potential

$$V_{cl}(v) \equiv -\mathcal{L}_0 = \frac{1}{2}(m^2 - \mu^2)v^2 + \frac{\lambda}{4}v^4$$
 (II.7)

The free propagator arises from the quadratic term L_2 in the fluctuating fields ϕ_1 and ϕ_2 . To derive the free propagator in the momentum space, we use the Fourier-Bessel transformation

$$\varphi_{i}(x) = \sqrt{\frac{\beta}{V}} \sum_{n,\ell,k} e^{i(\omega_{n}\tau + \ell\phi + k_{z}z)} J_{\ell}(k_{\perp}r) \tilde{\varphi}_{i}(k)$$
 (II.8)

with i = 1, 2. The cylindrical symmetry is implemented by introducing the cylinder coordinate system described by $x^{\mu} = (t, x, y, z) = (t, r \cos\phi, r \sin\phi, z)$, with r the radial coordinate, ϕ the azimuthal angle, and z the height of the cylinder. The conjugate momenta, corresponding to these coordinates at finite temperature T, are given by the bosonic Matsubara frequency $\omega n = 2\pi nT$, dis-crete quantum number ℓ , which is the eigenvalue of Lz, continuous momentum

 $k_{x'}$ and $k_{\perp} = |\mathbf{k}_{\perp}| = (k_x^2 + k_y^2)^{1/2}$ in cylindrical coordinates. The

Bessel function $J\ell$ (k, r) captures the radial dependence in this transformation and $\tau \equiv$ it. Plugging (II.8) into L₂ and performing an integration over cylindrical coordinates,

$$=\int_{X} \equiv \int_{0}^{2} d\tau \int_{0}^{\infty} r d\tau \int_{0}^{2\pi} d\phi \int_{-\infty}^{\infty} dz,$$
 (II.9)

we arrive after some manipulations at

$$\int_{X} \mathcal{L}_{2} = -\frac{V}{2} \sum_{n,\ell,k} (\bar{\varphi}_{1}(-k) \bar{\varphi}_{2}(-k)) (\beta^{2} \mathcal{D}_{\ell}^{-1}(k)) (\bar{\varphi}_{1}(k) \bar{\varphi}_{2}(k)), \qquad (II.10)$$

with the free propagator

$$\beta^{2} \mathcal{D}_{\ell}^{-1}(k) = \begin{pmatrix} \left(\omega_{n} + i\ell\Omega\right)^{2} + \omega_{1}^{2} - \mu^{2} & -2\mu\left(\omega_{n} + i\ell\Omega\right) \\ 2\mu\left(\omega_{n} + i\ell\Omega\right) & \left(\omega_{n} + i\ell\Omega\right)^{2} + \omega_{2}^{2} - \mu^{2} \end{pmatrix}$$
(II.11)

Here, $\omega_i^2 \equiv k^2 + m_i^2$, i = 1, 2, with $m_1^2(v) \equiv 3\lambda v^2$ + m^2 and $m_2^2(v) \equiv \lambda v^2 + m^2$, the corresponding masses to two fields φ 1 and φ 2. In cylinder coordinate system, we have $\mathbf{k}^2 \equiv \mathbf{k}_{\perp}^2 + \mathbf{k}_{\perp}^2$. In Sec. III, we break the global U(1) symmetry by choosing $m^2 = -c^2$ with $c^2 > 0$ and show that after considering the quantum corrections, ϕ^2 become a massless Goldstone mode.

A comparison with similar results for a nonrotating charged Bose gas at T and μ shows that while $\ell\Omega$ is said to play a role analogous to that of the chemical potential μ [23], the manner in which it is incorporated into the free propagator and the thermodynamic potential differs significantly (as discussed below).

B. The thermodynamic potential

To derive the thermodynamic potential V, corresponding to this model, we follow the standard procedure and define this potential by

$$V = -\frac{T}{V} \ln Z, \tag{II.12}$$

with

 $\ln \mathcal{Z} = -\frac{1}{2} \ln \det (\beta^2 \mathcal{D}_{\ell}^{-1}(k))$. (II.13) Let us first focus on $\ln \mathbb{Z}$

with Z the partition function of this model. Plugging $D\ell^{\text{-}1}$ from (II.11) into (II.13), we arrive first at

$$InZ = -\frac{1}{2} \sum_{e=\pm n,\ell,k} In \left| \beta^2 \left[\left(\epsilon_k^e \right)^2 + \left(\omega_n + i\ell\Omega \right)^2 \right] \right| \quad \text{(II.14)}$$

with $\epsilon_{\mathbf{k}}^{\pm}$ given by

$$\epsilon_k^{\pm} = \left(E_k^2 + \mu^2 + \sqrt{4\mu^2 E_k^2 + \delta M^4}\right)^{1/2},$$
 (II.15)

 $Ek^2 + M^2$ and

$$M^2 = \frac{1}{2}(m_1^2 + m_2^2), \quad \delta M^2 = \frac{1}{2}(m_1^2 - m_2^2).$$
 (II.16)

Following standard steps, it is possible to show that

$$\begin{split} & \ln \mathcal{Z} = -\frac{1}{4} \sum_{\mathbf{e} = \pm n, \ell, k} \Biggl\{ & \ln \Biggl(\beta^2 \Biggl[\omega_n^2 + \left(\epsilon_k^{\, \mathbf{e}} + \ell \Omega \right)^2 \Biggr] \Biggr) \\ & + & \ln \Biggl(\beta^2 \Biggl[\omega_n^2 + \left(\epsilon_k^{\, \mathbf{e}} - \ell \Omega \right)^2 \Biggr] \Biggr) \Biggr\} \end{split} \tag{II.17}$$

Performing the Matsubara sum with

$$\sum_{n=-\infty}^{+\infty} \ln((2\pi n)^2 + \eta^2) = \eta + 2\ln(1 - e^{-\eta})$$
 (II.18)

we arrive at

$$\begin{split} &\ln\mathcal{Z} = -\frac{V}{2} \sum_{\mathbf{e} = \pm} \int \int d\mathbf{k} \left\{ \beta \epsilon_{\mathbf{k}}^{\mathbf{e}} \right. \\ &\left. + \ln \left(\mathbf{1} - \mathbf{e}^{-\beta \left(\epsilon_{\mathbf{k}}^{\mathbf{e}} + \ell \Omega \right)} \right) + \ln \left(\mathbf{1} - \mathbf{e}^{-\beta \left(\epsilon_{\mathbf{k}}^{\mathbf{e}} - \ell \Omega \right)} \right) \right\} \end{split} \tag{II.19}$$

where the summation over k is replaced with the inte- gration over k in the cylinder coordinate system,

$$\sum_{k} \rightarrow V \sum_{x,l} \int d\vec{k}, \quad \text{with} \quad \int d\vec{k} \equiv \int \frac{k_{\perp} dk_{z}}{(2\pi)^{3}}.$$
 (II.20)

Here, $k \perp \equiv |\mathbf{k} \perp|$. Using (II.12), the thermodynamic potential V is given by

$$V = Vvac + VT,$$
 (II.21)

with the vacuum part

$$V_{\text{vac}} \equiv \frac{1}{2} \sum_{\ell} \int d\mathbf{k} \left(\mathbf{e}_{\mathbf{k}}^{+} + \mathbf{e}_{\mathbf{k}}^{-} \right), \tag{II.22}$$

and the matter (thermal) part

$$\begin{split} & \mathcal{V}_{T} = \frac{T}{2} \sum_{e=\pm} \sum_{\ell} \int d\vec{k} \left\{ \ln \left(1 - e^{-\beta \left(\varepsilon_{k}^{e} + \ell \Omega \right)} \right) \right. \\ & + \ln \left(1 - e^{-j \left(v_{0}^{\pm} \pm \Omega \right)} \right). \end{split} \tag{II.23}$$

Adding V with V_{cl} (v) from (II.7), to include the zero mode contribution, we obtain the full thermodynamic potential V_{tot},

$$\begin{split} &\mathcal{V}_{tot} = \frac{1}{2} (m^2 - \mu^2) V^2 + \frac{\lambda}{4} V^4 + \frac{1}{2} \sum_{\ell} \int d\vec{k} \left(\epsilon_{\vec{k}}^+ + \epsilon_{\vec{k}}^- \right) \\ &+ \frac{T}{2} \sum_{e = \pm \ell \neq 0} \tilde{\int} d\vec{k} \left\{ \ln \left(1 - e^{-\beta \left(\epsilon_{\vec{k}}^e + \ell \Omega \right)} \right) \right. \\ &+ \ln \left(1 - e^{-\beta \left(\epsilon_{\vec{k}}^e - \ell \Omega \right)} \right) \right\} \end{split} \tag{II.24}$$

C. Spontaneous breaking of global U(1) symmetry

Let us consider the classical potential (II.7). Assum- ing $m^2 > \mu^2$, the coefficient of v^2 in this expression is positive and, as it turns out, V_{cl} possesses one single min-imum at \overline{v}_0 =0 and the system is in its symmetric phase.

In this case, $m_1^2(v-o) = m_2^2(v-o) = m^2$, $\delta M^2 = o$ and ϵ_k^{\pm} is given by

$$\epsilon_k^{\pm} = \sqrt{k^2 + m^2} \mp \mu. \tag{II.25}$$

Here, m is a mass gap and $\Delta \epsilon \mathbf{k} = \epsilon \mathbf{k}^{-} - \epsilon \mathbf{k} = 2\mu \frac{1}{2}$. In Figur 1(a), ϵ \mathbf{k}^{+} e is plotted for generic mass m=1MeV and chemical potential $\mu = 0.6 \text{MeV} (\mu < \text{m})$

In the symmetry-broken phase characterized by $m^2 < \mu^2$, however, extremizing V_{cl} yields a maximum at va = 0 and two minima at

$$\frac{\overline{\nu}_5}{\sqrt{100}} = \pm \sqrt{\frac{\mu^2 - m_1^2}{\lambda}}.$$

The masses $m_1^2(v-b) = 3\mu^2 - 2m^2$ and $m_2^2(v-b) = \mu^2$. We thus have $M^2 = 2\mu^2 - m^2$ and $\delta M^2 = \mu^2 - m^2$ leading to

$$\epsilon_k^{\pm} = \sqrt{k^2 + (3\mu^2 - m^2)} \mp \sqrt{4\mu^2 k^2 + (3\mu^2 - m^2)}.$$
(II.26)

In Figure 1(b), $\in \frac{1}{k}$ is plotted for generic $\mu = 1.1 \text{MeV}$ and $m = 1MeV(\mu > m)$. As it is shown, whereas ϵk^- is quadratic in $k = |\mathbf{k}|, \epsilon \dot{\mathbf{k}} \sim 0$ for $k \sim 0$. This behavior indicates the presence of a massless Goldstone mode. By expanding $\epsilon_{\mathbf{k}}^{\pm}$ in the orders of $k \sim 0$, we obtain

$$\epsilon_k \simeq \sqrt{2(3\mu^2 - m^2)} + \frac{5\mu^2 - m^2}{2\sqrt{2(3\mu^2 - m^2)^3}} k^2,$$

$$r_{\kappa}^{\pm} \sim \sqrt{\frac{\mu^2 - m^2}{3\mu^2 - m^2}} |\kappa|.$$
 (II.27)

According to these results, $\epsilon_{\mathbf{k}}^{\scriptscriptstyle +}$ and $\epsilon_{\mathbf{k}^{\scriptscriptstyle -}}$ correspond to phonon and roton modes in the symmetry-broken phase $m < \mu$, respectively.

As it is shown in this section, $\ell\Omega$ appears in the thermal part of the effective potential VT from (II.23) and does not modify neither $k = |\mathbf{k}|, \epsilon \hat{\mathbf{k}} \sim 0$ nor the energy dispersion

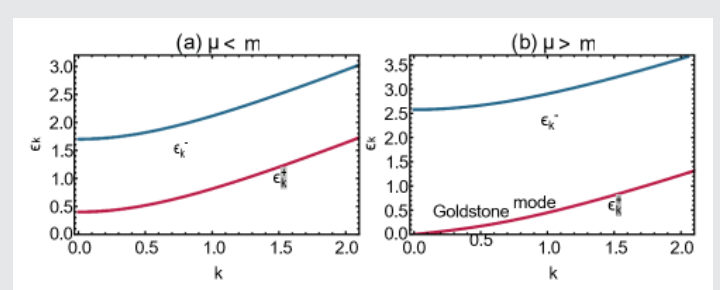


Figure 1: (color online). The k dependence of the energy dispersion $\epsilon_k^{\pm}k$ from (II.25) and (II.26) in the U(1) symmetric phase (panel a) and the symmetry-broken phase (panel b), characterized by μ < m and μ > m, respectively. As demonstrated, in the symmetry-broken phase, there is a massless Goldstone mode. These findings remain unchanged regardless of any rotation

 $\in \mathbf{k}^{\pm}$. Hence, a comparison with analogous results for nonrotating bosons [42] shows that rigid rotation has no effect on the behavior of j = 1; at $k \sim 0$.

D. Two special cases

In what follows, we consider two special cases $\lambda = 0, \mu \neq 0$ and $\neq 0, \mu = 0$:

Case 1: For the special case of noninteracting rotating Bose gas with $\lambda = 0$ and $\mu \neq 0$, we have $m_1 = m_2 = m$, $E_k^2 = \mathbf{k}^2 + m^2$ and $\delta M = o$. We thus have

$$\left. \epsilon_k^{\pm} \right|_{\lambda=0, \mu\neq 0} = \sqrt{\mathbf{k}^2 + \mathbf{m}^2} \mp \mu, \tag{II.28}$$

and therefore

$$V_{\text{tot}} \mid_{\lambda=0, \mu\neq 0} = \frac{1}{2} (m^2 - \mu^2) v^2 + \sum_{\ell} \int d\vec{k} \{E_k\}$$

$$+ T^{\left[\ln\left(1 - e^{-\beta(Ek - \mu eff)}\right) + \ln\left(1 - e^{-\beta(Ek + \mu eff)}\right)\right]^{\right]}}$$
(II.29)

with μ eff $\equiv \mu + \ell \Omega$. This potential is exactly the same potential arising in [30]. Using this potential, the effect of rotation on the BE condensation of a relativistic free Bose gas is studied.

Case 2: Another important case is characterized by

 $\lambda \neq 0$ and $\mu = 0$. In this case, $\in \mathbf{k}$ are given by

$$\epsilon_{\kappa}^{+} = \sqrt{\kappa^2 + m_2^2} = \omega_2,$$

$$\epsilon_{\kappa}^{-} = \sqrt{\vec{\kappa}^2 + m_1^2} = \omega.$$
(II.30)

Plugging (II.30) into (II.24) and choosing $\mu = 0$ and m² = $-c^2$ with $c^2 > 0$, the total thermodynamic potential is given by

Vtot
$$|\lambda \neq 0, \mu=0 = V_{cl} + V_{vac} + VT$$
, (II.31)

with the classical part

$$\mathcal{V}_{ci} = -\frac{\mathrm{e}^2 \gamma^2}{2} + \frac{\lambda v^4}{4},\tag{II.32}$$

the vacuum part

$$V_{\text{vac}} - \frac{1}{2} \sum_{\ell} \int dk \left(\omega_1 + \omega_2 \right), \tag{II.33}$$

and the thermal part

$$v_{\tau} = \frac{1}{2} \sum_{i=\beta} (v_i^+ - v_i^-), \qquad (II.34)$$

where

$$V_4^{\pm} = T \sum_{\ell \neq 0} \int_{k}^{\infty} k \ln \left(1 - e^{-\beta (\omega_{\ell} \mp \ell \dot{\mathbf{U}})} \right). \tag{II.35}$$

Here, ωi , i = 1, 2 are given in (II.30). Let us notice that in (II.35), the ℓ = 0 contribution is excluded, because the zero mode contribution is already captured by Vcl from (II.32). It is possible to limit the integration over ℓ

in V_T^{\pm} from (II.35). Having in mind that the arguments of $\ln(1-e^{-\beta(\omega i \ell\Omega)})$ are to be positive, the summation over ℓ in $\ln(1-e^{-\beta(\omega i - \ell\Omega)})$ is over $\ell \in (-\infty, -1]$ and in $\ln(1 - e^{-\beta(\omega i + \ell\Omega)})$ is over $\ell \in [1, \infty)$ [30]. Performing a change $\ell \to -\ell$, we thus

$$\mathcal{V}_{i}^{+} = T \sum_{l=1}^{\infty} \int d\overline{k} \ln \left(1 - e^{-\beta(\omega_{l} + \ell \dot{\mathbf{U}})} \right) = \mathcal{V}_{i}^{-}. \tag{II.36}$$

Hence, the final form of VT from (II.34) reads

$$V_{T} = T \sum_{i=1,2} \sum_{\ell=1}^{\infty} \int d\overline{k} \ln \left(1 - e^{-\beta(\omega_{i} + \ell \dot{\mathbf{U}})} \right). \tag{II.37}$$

III. Spontaneous breaking of global U(1) symmetry in a rigidly rotating bose gas

A. The critical temperature of U(1) phase transition; **Analytical result**

In this section, we study the effect of rigid rotation on the spontaneous breaking of global U(1) symmetry in an interacting charged Bose gas. Before starting, we add a new term

$$\tilde{Z}_0 = \frac{1}{2} n_0^2 (\varphi_1 + v) v,$$
 (III.1)

to L from (II.5). This leads to an additional mass term in the classical potential Vcl. We define a new mass

 $a^2 \equiv c^2 + m_0^2$, which replaces c^2 in (II.32). Minimizing the resulting expression, the (classical) minimum of V_{cl} is thus given by

$$V_0^2 = \frac{a^2}{\lambda}.$$
 (III.2)

At this minimum, the masses of $m_1^2(v) = 3\lambda v^2 - c^2$ and $m_2^2(v) = \lambda v^2 - c^2$ are given by

$$m_1^2(v_0) = 3a^2 - c^2, m_2^2(v_0) = a^2 - c^2$$
 (III.3)

For $m_0 = 0$, we have $m_2 = 0$ and $\varphi 2$ becomes a massless Goldstone mode. The position of this (classical) mini- mum changes, once the contribution of the thermal part of the thermodynamic potential, VT, is considered. To show this, we first define $V_a \equiv V_{cl} + VT$ and use the high-temperature expansion of VT by making use of the results presented in Appendix A. Considering only the first two terms of (A.13)

and plugging the definitions oof $m_1^2(v)$ and $m_1^2(v)$ into it, the high-temperature expansion of V₂ reads

$$\mathcal{V}_{a}(v,T,\Omega) = -\frac{a^{2}v^{2}}{2} \left(1 - \frac{2\lambda T^{3}\zeta(3)}{a^{2}\pi^{2}\Omega}\right) + \frac{\lambda v^{4}}{4} - \frac{2T^{5}\zeta(5)}{\pi^{2}\Omega} - \frac{c^{2}T^{3}\zeta(3)}{2\pi^{2}\Omega} + \cdots$$
(III.4)

Setting the coefficient of v² equal to zero, the critical tem-perature of global U(1) phase transition is determined,

$$Tc = \left(\frac{a^2 \pi^2 \Omega}{2\lambda \zeta(3)}\right)^{1/3}$$
 (III.5)

In [30], the BE transition in a noninteracting Bose gas

under rigid rotation is studied. It is shown that in nonrelativistic regime $Tc \propto \Omega^{2/5}$ and in ultrarelativistic regime Tc $\propto \Omega^{1/4}$. In the present case of interacting Bose gas, similar to that noninteracting cases, the critical temper- ature increases with increasing Ω .

Introducing the reduced temperature t = T/Tc, with Tc = Tc (Ω) from (III.5), and minimizing Va from (III.4) with respect to v, the new nontrivial minimum is given by

$$v_{min}^{2}(T,\Omega) = \begin{cases} \frac{a^{2}}{\lambda}(1-t3)'t < 1, \\ (0,t \ge 1) \end{cases}$$
 (III.6)

When comparing with a similar result for a nonrotating charged Bose gas [40], it turns out that the power of t in (III.6) changes once the gas is subjected to small rotation. In Sec. IV, we numerically study the effect of rotation on the spontaneous breaking of global U(1) symmetry. For this purpose, we employ a phenomenological model that includes σ and π mesons, replacing ϕ 1 and ϕ 2 fields in the above computation. We set $m_1^2(v_0) = 3\lambda v_0^2 - c^2 =$ $\rm m_\sigma^2$ and $\rm m_2^2 \left(v_0 \right) = \lambda v_0^2 - c^2 = m_\pi^2$ with $\rm V_0$ the classical minimum from (III.2). Moreover, we choose mo in (III.1) equal to $m\pi$. For m_g=400MeV and m_g=140MeV, we obtain

$$c = \left(\frac{m_{\sigma}^2 - 3m_{\pi}^2}{2}\right) 1/2 \simeq 225 \text{ MeV}.$$
 (III.7)

Moreover, $a = (c_2 + m_\pi^2)^{1/2} \approx 265 \text{MeV}$. We also choose $\lambda = 0.5$. Using these quantities the function

$$\Delta Va \equiv Va (v, T,\Omega) - Va (0, T,\Omega)$$

$$= -\frac{a^2 v^2}{2} (1 - t3) + \frac{\lambda v^4}{4}, \qquad (III.8)$$

is plotted in Figure 2 at t = 0.6, 0.8 in the symmetrybroken phase and t = 1.2 in the symmetry-restored phase. At t = 1 a phase transition from the symmetry-broken phase to a symmetry-restored phase occurs. Let us notice, that the effect of rotation consists of changing the power of t in (III.6) and (III.8) from t² to t³. This is apart from the Ω dependence of the critical temperature Tc from (III.5) (Figure 7).

The result indicates a continuous phase transition from a symmetry-broken phase at t < 1 to a symmetry- restored phase at $t \ge 1$. To scrutinize this conclusion, let us consider the pressure P arising from Va from (III.4).

It is given by P = -Va. Denoting the pressures below and above Tc with P< (v, T,Ω) and P> (v, T,Ω) , we have P<

$$P_{<}(vmin,T,\Omega) = -\frac{a^4}{2\lambda}t^3 + \frac{c^2T^3\zeta(3)}{2\pi^2\Omega} + \frac{2T^5\zeta(5)}{\pi^2\Omega} + \frac{a^4}{4\lambda}t^6,$$

$$P > (0,T,\Omega) = \frac{c^2T^3\zeta(3)}{2\pi^2\Omega} + \frac{2T^5\zeta(5)}{\pi^2\Omega} - \frac{a^4}{\lambda\lambda}$$
 (III.9)

Here, we have added a term $-a^4/4\lambda$ to P< and P> in order to guarantee $P_{<}\begin{pmatrix} 2^2 \\ V_{min}, 0, \Omega \end{pmatrix} = 0$ and $P_{<} = P_{>}$ at the the transition temperature T_c . At $T = T_c$, the pressure is

$$P_{c}(v_{\min}^{2}, T_{c}, \Omega) = P_{c}(0, T_{c}, \Omega)$$

$$= -\frac{a^{4}}{4\lambda} + \frac{a^{2}c_{z}^{2}}{4\lambda} + \frac{a^{10}\pi^{4}\Omega^{2}\zeta(5)}{2^{2}\Lambda^{5}[\zeta(3)]^{5}}$$
(III.10)

For m0 = 0 (or a = c), the first two terms cancel, resulting in an increase in pressure as Ω increases. Moreover, whereas the entropy (dP/dT) is continuous at

$$T = Tc, \frac{dP_{<}}{dT}\Big|_{Tc} = \frac{dP_{>}}{dT}\Big|_{Tc}$$
 (III.11)

the heat capacity $(d^{2}P/dT^{2})$ is discontinuous

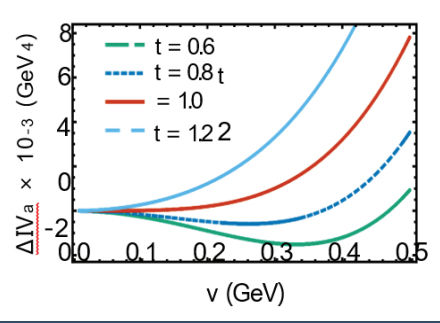


Figure 2: (color online). The v dependence of ΔVa from (III.8) is plotted at t = 0.6, 0.8, 1, 1.2. At t < 1 the global U(1) symmetry is broken and ΔVa possesses nontrivial minima at $v_{min}^2 = a^2 (1 - t^3)/\lambda$. At t = 1 the symmetry is restored and at $t \ge 1$ a single minimum at v_{min} = 0 appears (see (III.6))



$$\frac{d^{2}P_{<}}{dT^{2}}\mathbf{I}_{\tau_{c}} - \frac{d^{2}P_{>}}{dT^{2}}\mathbf{I}_{\tau_{c}} = \frac{9c^{8/3}[\zeta(3)]^{2/3}}{2^{1/3}\pi^{4/3}\lambda^{1/3}\Omega^{2/3}}$$
(III.12)

Hence, according to Ehrenfest classification, this is a sec- ond order phase transition. In comparison to the non-rotating case [40], although rotation alters the critical temperature, the order of the phase transition remains unchanged. It is noteworthy that the discontinuity in the heat capacity decreases with increasing Ω .

Plugging at this stage, winn from (III.6) into $m_1^2(v) = 3\lambda v^2 - c^2$ and $m_2^2(v) = \lambda v^2 - c^2$, we arrive at

$$\begin{split} m_1(\text{vmin}) &= 3 - a^2 \left(1 - t^3\right) - c^2, & t < 1 \\ c^2, & t \geq 1 \\ m_2(\text{vmin}) &= & a^2 \left(1 - t^3\right) - c^2, \\ -c^2, & t < 1 \end{split}$$
 (III.13)

Hence, as it turns out, at $t \ge 1$, after the symmetry is restored, m_1^2 and m_2^2 become negative. Contrary to our expectation, for a = c, i.e., in the chiral limit m0 = 0, the Goldstone boson '2 acquires a negative mass $-c^2t^3$ in the symmetry-broken phase at t < 1. In what follows, we compute the one-loop tadpole diagram contributions to masses m1 and m2. We show, in particular, that by considering the thermal mass, the one-loop corrected mass of the Goldstone mode '2 vanishes in chiral limit m0 = 0.

B. One-Loop Corrections to m¹ (v) and m² (v)

To calculate the one-loop corrections to $\boldsymbol{m}_{_{1}}$ and $\boldsymbol{m}_{_{2}}\text{, let}$ us consider L₄ from (II.4). Three vertices, corre-sponding to three terms in $\mathcal{L}_{\mathbf{L}} = -\frac{\lambda}{L} \left(\varphi_{\mathbf{1}}^2 + \varphi_{\mathbf{2}}^2 \right)^2$, are to be considered in this computation (Figure 3),

They lead to two different tadpole contributions to $\langle \Omega \mid T('1(x)'1(y)) \mid \Omega \rangle$ and $\langle \Omega \mid T('2(x)'2(y)) \mid \Omega \rangle$ that correct m_1 and m_2 perturbatively. They are denoted by Πij with the first index, i = 1; 2, corresponds to whether '1 or '2 are in the external legs, and the second index j = 1;2 to whether the internal loop is built from '1 or '2 (Figure 4, where $\Pi i j$ are plotted). Hence, according to this notation, the one-loop perturbative corrections to m_1^2 and m_2^2 arise

$$\begin{split} & \text{m}_1^2(v) \to \text{m}_1^2(v) + \Pi 11 + \Pi 12; \\ & \text{m}_2^2(v) \to \text{m}_2^2(v) + \Pi 21 + \Pi 22 \; . \end{split} \tag{III.15}$$

At this stage, we introduce

$$\Pi(T,\Omega,m_i) = T \sum_{n=-\infty}^{\infty} \sum_{\ell=-\infty}^{\infty} \int d\vec{k} D_{\ell}(\omega_n,\omega_i)$$
 (III.16)

with free boson propagator

$$D_{\ell}(\omega_n, \omega_i) = \frac{1}{(\omega_n - i\ell\Omega)^2 + \omega_i^2}$$
 (III.17)

arising from (II.11) with = 0. Here, $l_i^2 = k_{\perp}^2 + k_{Z}^2 + m_i^2$ and i =1; 2. Using this notation, it turns out that

$$\Pi \ 11 = 3\Pi \ 1 \ ; \Pi \ 12 = \Pi 2 \ ;$$

$$\Pi \ 22 = 3\Pi \ 2 \ ; \Pi \ 21 = \Pi \ 1. \ (III.18)$$

Hence, the perturbative corrections of masses are given

$$\begin{aligned} & \text{m}_2^2(\text{v}) \rightarrow \text{m}_2^2(\text{v}) + 3\Pi_2 + \Pi_1 \\ & \text{m}_2^2(\text{v}) \rightarrow \text{m}_2^2(\text{v}) + 3\Pi_2 + \Pi_1 \end{aligned} \tag{III.19}$$

To evaluate Π_i from (III.16), we follow the same steps as presented in [30]. The Matsubara summation is eval-2 uated with

$$\sum_{n} D_{\ell} \left(\omega_{n}, \omega_{i} \right) = \frac{1}{2T\omega_{i}} \left[n_{b} \left(\omega_{i} + \ell\Omega \right) + n_{b} \left(\omega_{i} - \ell\Omega \right) + 1 \right]$$
(III.20)

where $n_b(!) \equiv 1 = (e\beta\omega - 1)$ is the BE distribution func-

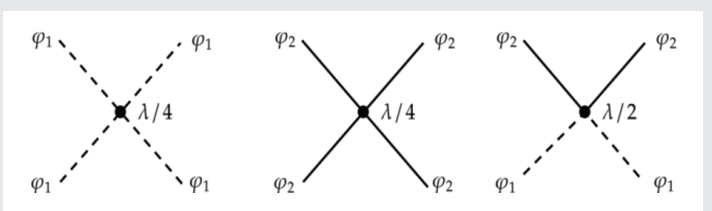


Figure 3: Three vertices arising from L4 from (II.4). Dashed and solid lines correspond to $\phi 1$ and $\phi 2$ fields, respectively.

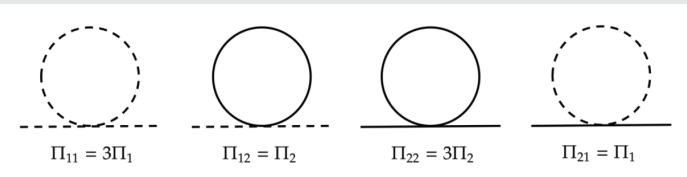


Figure 4: The tadpole diagrams contributing to the one-loop corrections of m₁² and $m_{_{2}}^{2}$. Dashed and solid lines correspond to $\phi 1$ and $\phi 2$ fields, respectively.

tion. In what follows, we insert (III.20) into (III.16) and focus only on the matter (T and Ω dependent) part of

Πi,
$$\Pi_{i}^{mat} = \frac{1}{2} \sum_{e=\pm} \sum_{\ell \neq 0} \int d\tilde{k} \frac{n_b(\omega_i + e\ell\Omega)}{\omega_i}$$
. (III.21)

Having in mind that in $nb(!i \pm '\Omega)$, we must have $e\beta(\omega i \pm \ell\Omega) - 1 > 0$, it is possible to limit the summation over. We thus obtain $\Phi_{i}^{i}^{\mathrm{mathrm}\{mat\}}=\sum_{i}^{mathrm}$ ell=1}^{\infty} \int d \tilde{k} \frac{n_{b}\left(\omega_ {i}+\ell \Omega\right)}{\omega_{i}}\$.

Let us notice that in the term including nb (! i Ω) an additional shift \rightarrow - is performed. To carry out the summation over `and eventually the integration over k_ and k₂, we use

$$n_b(\omega_i + \ell\Omega) = T \frac{d}{d\omega_i} ln \left(1 - e^{-\beta(\omega_i + \ell\Omega)}\right)$$
 (III.23)

and arrive first at

$$\Pi_{j}^{\text{mat}} = T \sum_{\ell=1}^{\infty} \int d\tilde{k} \frac{1}{\omega_{j}} \frac{d}{d\omega_{j}} \ln \left(1 - e^{-\beta \left(\omega_{j} + \ell \Omega \right)} \right)$$
 (III.24)

Using, at this stage, (A.2), we then obtain

$$\Pi_{i}^{\text{mat}} = -T \sum_{\ell=1}^{\infty} \sum_{j=1}^{\infty} \int d\vec{k} \frac{1}{\omega_{i}} \frac{d}{d\omega_{i}} \frac{e^{-\beta\omega_{i}j} e^{-\beta\ell\Omega j}}{j}$$

$$=\sum_{\ell=1}^{\infty}\sum_{j=1}^{\infty}\int d\vec{k}\,\frac{e^{-\beta\omega_{j}}\,e^{-\beta\Omega_{\ell j}}}{\omega_{\ell}} \tag{III.25}$$

The summation over `can be performed by making use of (A.4). Assuming Ω < 1 and using (A.5), Π i(mat)i reads

$$\Pi_{i}^{\text{mat}} = \frac{1}{\Omega} \sum_{i=1}^{\infty} \frac{1}{j} \int d\vec{k} \frac{e^{-\beta \omega_{i,j}}}{\omega_{i}}$$
 (III.26)

Following the method presented in Appendix B, we finally arrive at

$$\Pi_i^{\text{mat}} = \frac{\lambda T^3 \zeta(3)}{2\pi^2 \Omega} + \cdots$$
 (III.27)

The first term in (III.27) is analogous to the thermal mass λT² /3 in a nonrotating interacting Bose gas [40] and the ellipsis includes higher order corrections of Πi(mat)i in βmi.

At high temperature, it is enough to consider only the first term in (III.27), which is independent of mi. We thus have

$$\Pi_{1}^{\text{mat}} = \Pi_{2}^{\text{mat}} = \frac{\lambda T^{3} \zeta(3)}{2\pi^{2} \Omega}$$
 (III.28)

and therefore

$$\begin{split} P_{<}(\text{vmin},T,\Omega) &= -\frac{a^4}{2\lambda}t^3 + \frac{c^2T^3\zeta(3)}{2\pi^2\Omega} + \frac{2T^5\zeta(5)}{\pi^2\Omega} + \frac{a^4}{4\lambda}t^6, \\ P_{>}(0,T,\Omega) &= \frac{c^2T^3\zeta(3)}{2\pi^2\Omega} + \frac{2T^5\zeta(5)}{\pi^2\Omega} - \frac{a^4}{\lambda\lambda} \end{split}$$
 (III.29)

with t = T/Tc and Tc from (III.5).

C. Goldstone theorem

Let us consider again the result presented in (III.13). Adding the contribution of thermal mass (III.28) to $m_1^2(v_{min}^2)$ and $m_2^2(v_{min}^2)$, according to (III.29), we obtain

$$m_{1}^{2}(v_{min}) = \begin{cases} 2c^{2}(1-t^{3})+3m_{0}^{2}\left(1-\frac{2t^{3}}{3}\right), & t<1, \\ c^{2}(t^{3}-1)+m_{0}^{2}t^{3}, & t\geq1, \end{cases}$$

$$m_{2}^{2}(v_{min}) = \begin{cases} m_{0}^{2}, & t<1, \\ c^{2}(t^{3}-1)+m_{0}^{2}t^{3}, & t\geq1, \end{cases}$$
(III.30)

where $a^2 = c^2 + m_0^2$ is used. Assuming $m_0 = 0, m_2$ vanishes at t < 1. This indicates that the Goldstone theorem is valid when the thermal mass corrections to m_1^2 and m_2^2 are taken into account. Moreover, we observe that $m_1^2(vmin) = m_2^2(vmin)$ in the symmetry-restored phase at $t \ge 1$. In Figure 5, the t dependence of m_1^2 vmin and m_2^2 vmin from (III.30) is plotted. These masses are identified with m_{σ}^{2} and m_{π}^{2} , respectively. We use $c \approx 0.225$ GeV from (III.7) and mo = 0.140GeV , as de-scribed in Sec. III B and observe that in the symmetry- broken phase, at $t < 1, m_{\sigma}$ decreases with increasing temperature, while $m\pi$ remains constant. As expected, at symmetry-restored phase at $t \ge 1, m_{\sigma}$ and $m\pi$ are equal and increase with increasing temperature. It is noteworthy that the effect of rotation, apart from affect- ing the value of

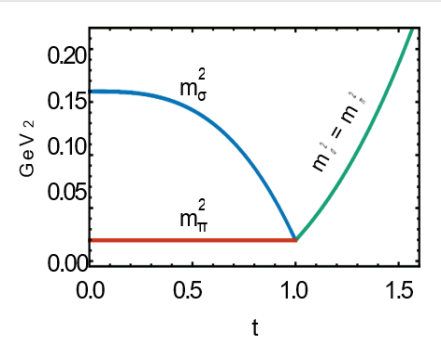


Figure 5: (color online). The t dependence of m₁² and m₂²2 from (III.30) at vm(2)min from (III.6) is plotted. These masses are iden-tified with σ and π meson masses. In the symmetry-broken phase, at t < 1, mσ decreases with increasing temperature, while $m\pi$ remains constant. At symmetry-restored phase at $t \ge 1$, $m\sigma$ and $m\pi$ are equal and increase with increasing t

the critical temperature Tc from (III.5), consists of changing the power of t in (III.30) from t^2 to t^3 (see [40]).

D. Vacuum potential

In what follows, we compute the contribution of the vacuum part of the thermodynamic potential, Vvac from (II.33) to Vtot. Let us first consider the summation over $\ell \in$ $(-\infty, +\infty)$ in this expression. This sum is divergent and need an appropriate regularization. To perform the summation over ℓ, we use

$$\sum_{\ell=-\infty}^{\infty} 1 = \lim_{x\to 0} \sum_{\ell=-\infty}^{\infty} e^{-\ell^2 x}$$

$$= \lim_{x \to 0} \left(1 + 2 \sum_{\ell=1}^{\infty} e^{-\ell^2 x} \right) = 1 + \lim_{x \to 0} \frac{1}{1 - e^{-x}}$$

Neglecting the divergent term, we obtain

$$V_{\text{vac}} = \frac{1}{2} \int d\vec{k} \left(\omega_1 + \omega_2 \right)$$
 (III.32)

The above regularization guarantees that rotation does not alter Vvac. To perform the integration over k⊥ and kz, let us consider the integral

$$I(m) = \frac{\overline{\mu}^{\varepsilon}}{2} \int d\tilde{k} \left(k^2 + m^2 \right)^{1/2}$$
 (III.33)

with $\epsilon = 3$ -d. Here, d is the dimension of spacetime and $\overline{\mu}$ denotes an appropriate energy scale. Later, we show that $\overline{\mu}$ can be eliminated from the computation. Utilizing

$$\Phi(m,d,n) = \int \frac{d^{d}k}{(2\pi)^{d}} \frac{1}{\left(k^{2} + m^{2}\right)^{n}}$$

$$= \frac{1}{(4\pi)^{d/2}} \frac{\Gamma(n-d/2)}{\Gamma(n)} \frac{1}{\left(m^{2}\right)^{n-d/2}}$$
(III.34)

to perform a d dimensional regularization, we obtain for $\Phi(m,3 - \epsilon,-1/2)$, (In Appendix C, we derive (III.24) in cylinder coordinate system).

$$I(m) = -\frac{m^4}{64\pi^2} \left(\frac{2}{\varepsilon} + \frac{3}{2} - \gamma_{\varepsilon} - \ln \left(\frac{m^2}{4\pi u^2} \right) \right)$$
 (III.35)

The vacuum part of the thermodynamic potential (III.32) is thus given by

$$Vvac = I(m1) + I(m2)$$

$$= -\frac{m_1^4 + m_2^4}{64\pi^2} \left(\frac{2}{\varepsilon} + \frac{3}{2} - \gamma_E\right) + \frac{m_1^4}{64\pi^2} \ln\left(\frac{m_1^2}{4\pi\mu^2}\right) + \frac{m_2^4}{64\pi^2} \ln\left(\frac{m_2^2}{4\pi\mu^2}\right)$$
(III.36)

In what follows, we regularize this potential by following the method presented in [43]. To do this, we first define

$$Vb \equiv V_{cl} + V_{vac} + VCT, \qquad (III.37)$$

with V_{cl} from (II.32) with c^2 replaced with $a^2 = c^2 + m_0^2$ and V_{vac} from (III.36). The counterterm potential is given by

$$\mathcal{V}_{CT} = \frac{Av^2}{2} + \frac{Bv^4}{A} + C \tag{III.38}$$

The coefficients A and B are determined by utilizing two prescriptions

$$\frac{\partial \mathcal{V}_b}{\partial \mathbf{v}}\Big|_{\mathbf{v}_0^2} = \mathbf{0}, \quad \frac{\partial^2 \mathcal{V}_b}{\partial \mathbf{v}^2}\Big|_{\mathbf{v}_0^2} = m_1^2(\mathbf{v}_0)$$
 (III.39)

Here, v_0^2 from (III.2) is the classical minimum and m_1^2 (vo) from (III.3). Let us note that the first prescription guar- antees that the position of the classical minimum does not change by considering the vacuum part of the poten-tial. The term C in (III.38) includes all terms which are independent of v. Using (III.39), we arrive at

$$A = -\frac{m_0^2}{2} + \frac{3c^2\lambda}{8\pi^2} + \frac{c^2\lambda\gamma_E}{4\pi^2} + \frac{5m_0^2\lambda}{8\pi^2} - \frac{c^2\lambda}{2\pi^2\varepsilon}$$

$$+\frac{c^2\lambda}{16\pi^2}ln\!\!\left(\frac{m_0^2}{4\pi\overline{\mu}^2}\right)\!\!+\!\frac{3c^2\lambda}{16\pi^2}ln\!\!\left(\frac{2c^2+3m_0^2}{4\pi\overline{\mu}^2}\right)$$

$$B = \frac{m_0^2 \lambda}{2a^2} - \frac{5\lambda^2 \gamma_E}{8\pi^2} + \frac{5\lambda^2}{4\pi^2 \varepsilon} - \frac{\lambda^2}{16\pi^2} \ln \left(\frac{m_0^2}{4\pi\mu^2} \right)$$

$$-\frac{9\lambda^2}{16\pi^2}\ln\left(\frac{2c^2+3m_0^2}{4\pi\tilde{\mu}^2}\right) \tag{III.40}$$

Plugging A and B from (III.40) into VCT from (III.38) and choosing

$$C = \frac{c^4}{16\pi^2 \varepsilon} - \frac{c^4}{64\pi^2} \ln \left(\frac{m_0^2}{4\pi\mu^2} \right) - \frac{c^4}{64\pi^2} \ln \left(\frac{2c^2 + 3m_0^2}{4\pi\mu^2} \right)$$

$$+\frac{3c^4}{64\pi^2} - \frac{c^4\gamma_E}{32\pi^2}$$
 (III.41)

vthe counterterm potential from (III.38) is determined. These counterterms eliminate the divergent terms in the vacuum potential, as expected. The total potential Vb from (III.37) is thus given by

$$V_b = -\frac{a^2 v^2}{2} + \frac{\lambda v^4}{\Delta} - \frac{m_{\phi}^2 v^2}{\Delta} + \frac{3c^2 \lambda v^2}{8\pi^2} + \frac{5m_{\phi}^2 \lambda v^2}{16\pi^2}$$

$$-\frac{15\lambda^{2}v^{4}}{64\pi^{2}} + \frac{m_{0}^{2}\lambda v^{4}}{8\alpha^{2}} + \frac{m_{1}^{4}}{64\pi^{2}} ln \left(\frac{m_{1}^{2}}{2c^{2} + 3m_{0}^{2}}\right) + \frac{m_{2}^{4}}{64\pi^{2}} ln \left(\frac{m_{2}^{2}}{m_{0}^{2}}\right)$$
(III.42)

As mentioned earlier, the energy scale $\bar{\mu}$ does not appear in the final expression of Vb. Additionally, a nonzero m0 is necessary to specifically regularize the last term in Vb from (III.42).

E. Ring potential

We finally consider the nonperturbative ring potential Vring. As mentioned in the previous paragraphs, the Lagrangian is written in terms of φ 1 and φ 2, three type of vertices appear in the $\lambda(\phi \star \phi)$ model (Figure 3). We thus have four different types of ring diagrams:

- Type A: A ring with N insertions of $\Pi 2$ and N propagators D ℓ (ω n, ω 1) propagators, V^{A}_{ring}
- Type B: A ring with N insertions of Π 1 and N propagators $D\ell$ ($\omega n, \omega 2$) propagators, V_{rino}^{B}
- Type C: A ring with r insertions of $\Pi 2$ and s insertions of Π 1 with N propagators $D\ell$ ($\omega n, \omega 2$), V_{ring}^{C} .

Here, $r \ge 1$ and r + s = N.

Type D: A ring with r insertions of Π 1 and s inser \mathbb{Z} tions of $\Pi 2$ with N propagators $\mathrm{D}\ell$ ($\omega \mathrm{n}, \omega$ 1), V^D ring.

Similar to the previous case, $r \ge 1$ and r + s = N.

Here, Πi ($T_i\Omega_i$, mi) and $D\ell$ ($\omega n_i\omega i$), i=1,2 are defined in (III.16) and (III.17), respectively. In Figure 6, these different types of ring potentials are demonstrated. The If full contribution of the ring potential is given by

$$V_{\text{ring}} = \sum_{l=\{A,\dots,D\}} V_{\text{ring}}^{l}$$
(III.43)

Following standard field theoretical method, it is possible to determine the combinatorial factors leading to the standard form of the ring potential [40]. In Appendix D, we outline the derivation of V_{ring}^{I} , I = A, ..., D. They are given by

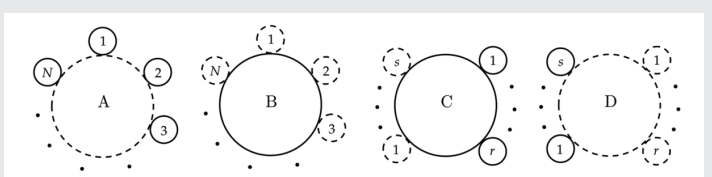


Figure 6: Ring diagrams of Type A, B, C, and D contributing to the nonperturbative ring potential Vring. Dashed and solid lines correspond to $\phi 1$ and $\phi 2$, respectively They are given by the expressions from (III.44).

$$\mathcal{V}_{ring}^{A} = -\frac{T}{2} \sum_{n,\ell} \int dk \sum_{N=2}^{\infty} \frac{1}{N} (-\Pi_{2}D_{1})^{N}, \\
\mathcal{V}_{ring}^{B} = -\frac{T}{2} \sum_{n,\ell} \int dk \sum_{N=2}^{\infty} \frac{1}{N} (-\Pi_{1}D_{2})^{N}, \\
\mathcal{V}_{ring}^{C} = -\frac{T}{2} \sum_{n,\ell} \int dk \sum_{N=2}^{\infty} \sum_{r=1}^{N} \frac{(N-r)!(r-1)!}{N!} \\
\times \left[(-D_{2})^{\Gamma} (-\Pi_{1})^{N} - r^{\Gamma}D_{2}^{N}, \right] \\
\mathcal{V}_{ring}^{D} = -\frac{T}{2} \sum_{n,\ell} \int dk \sum_{N=2}^{\infty} \sum_{r=1}^{N} \frac{(N-r)!(r-1)!}{N!} \\
\times \left[(-\Pi_{1})^{r} (-\Pi_{2})^{N-r} D_{1}^{N} \right] \tag{III.44}$$

Here, the notation $Di \equiv D\ell (\omega n, \omega i)$ is used. To evaluate V_{ring}^{A} and V_{ring}^{B} , we introduce a simplifying notation

$$\mathcal{V}_{\text{ring}}^{(i,j)} = -\frac{T}{2} \sum_{n,i} \int d\tilde{k} \sum_{N=2}^{\infty} \frac{1}{N} \left(-\Pi_i D_j\right)^N$$
 (III.45)

Here, (i, j) = (2, 1) and (i, j) = (1, 2) correspond to Vr(A)ring and V_{ring}^{B} , respectively. Plugging Dj from (III.17) into (III.45) and focusing on n = 0 as well as $\ell \neq 0$ contributions in the summation over n and ℓ , we arrive first at

$$V_{\text{ring}}^{(i,j)} = T \sum_{k=1}^{\infty} \int d\vec{k} \sum_{N=2}^{\infty} \frac{(-1)^{N+1}}{N} (u_j^2)^{-N} (\Pi_i)^N$$
 (III.46)

with
$$u_{\boldsymbol{i}}^2 \equiv k_{\perp}^2 + k_{Z}^2 + m_{\boldsymbol{i}}^2 - \ell^2 \Omega^2$$
. Plugging then

$$(k_{ij}^{2})^{-N} = \frac{1}{\Gamma(N)} \int_{0}^{\infty} dt \ t^{N-1} e^{-m^{2}t} e^{-(k_{1}^{2} + k_{2}^{2})t} e^{e^{2}\Omega^{2}t}$$
(III.47)

into (III.46), the integration over k⊥ and kz can be car- ried out by making used of (A.9). To limit the summation over ℓ from below, we use the fact that the summand is even in ℓ . To perform the integration over $k\perp$ and kz, we use the Mellin transformation of $\left(u_{\mathbf{i}}^{2}\right)-N$

$$(u_{ij}^{2})^{-N} = \frac{1}{\Gamma(N)} \int_{0}^{\infty} dt \ t^{N-1} e^{-m^{2}t} e^{-(k_{1}^{2} + k_{2}^{2})t} e^{e^{2}\Omega^{2}t}$$
(III.48)

and (A.9) to arrive first at

$$\mathcal{V}_{\text{ring}}^{(i,j)} = \frac{T}{8\pi^{3/2}} \sum_{N=2}^{\infty} \frac{(-1)^{N+1} \prod_{i}^{N}}{N \Gamma(N)} \int_{0}^{\infty} dt \ t^{N-5/2} e^{-m_{j}^{2}t} I(\Omega)$$
(III.49)

where



$$I(\Omega) \equiv \sum_{t=1}^{\infty} e^{t^2 \Omega^2 t}$$
 (III.50)

To evaluate the summation over ℓ , we expand $e^{\ell 2} \Omega^2 t$ in a Taylor expansion and obtain

$$I(\Omega) = \sum_{r=0}^{\infty} \frac{(\Omega^2 t)^r}{r!} \zeta(-2r)$$
 (III.51)

with

 $\sum_{r=0}^{\infty}\ell^{2r} = \zeta(-2r), \quad \zeta(z)$ the Riemann zeta function. Since

for $r \in N$, we have $\zeta(-2r) = 0$, the only nonvanishing contribution to the summation over r arises from r = o. We thus use $\zeta(\mathbf{0}) = -\frac{1}{2}$ to arrive at

$$I(\Omega) = -\frac{1}{2}$$
 (III.52)

Plugging this result into (III.49), using

$$\int_0^\infty dt \ t^{N-\frac{5}{2}} e^{-m_j^2 t} = (m_j^2)^{-(N-\frac{3}{2})} \Gamma(N-\frac{3}{2})$$
 (III.53)

and performing the summation over N, we arrive at

$$V_{\text{ring}}^{(i,j)} = \frac{T}{24\pi} \left[2(m_j^2 + \Pi_i)^{3/2} - 2m_j^3 - 3m_j \Pi_i \right]$$
 (III.54)

We arrive eventually at

$$A V_{ring} = V_{ring}^{\begin{pmatrix} 2 \\ 1 \end{pmatrix}}, V_{ring} = V_{r}^{\begin{pmatrix} 1 \\ in \end{pmatrix}}, (III.55)$$

To evaluate V_{ring}^{c} and V_{ring}^{D} , we introduce

$$V_{\text{ring}}^{(i,j)} = -\frac{7}{2} \sum_{n,\ell} \int d\vec{k} \sum_{N=2}^{\infty} \sum_{r=1}^{N} \frac{(-1)^{N} (N-r)! (r-1)!}{N!}$$

$$V_{ring}^{(i,j)} = -\frac{7}{2} \sum_{n,\ell} \int d \tilde{k} \sum_{N=2r=1}^{N} \frac{(-1)^{N} (N-r)! (r-1)!}{N!} \times \prod_{\mathbf{i}}^{r} \prod_{\mathbf{i}}^{N} -r^{N} D_{\mathbf{i}}^{N}$$
(III.56)

Here, (i, j) = (2, 1) corresponds to V_{ring}^{c} and (i, j) = (1, 2)to V_{ring}^{D} . Plugging Di from (III.17) into (III.56) and fo cusing on n = 0 and $\ell \neq 0$ contributions in the summation over n and ℓ , we obtain

$$V_{\text{ring}}^{(i,j)} = T \sum_{\ell=1}^{\infty} \int d\vec{k} \sum_{N=2}^{\infty} \sum_{r=1}^{N} \frac{(-1)^{N} (N-r)! (r-1)!}{N!}$$

$$\times \prod_{i=1}^{r} \prod_{j=1}^{N-r} (u_{i}^{2})^{-N}$$
(III.57)

where $u_{\boldsymbol{i}}^2$ is defined below (III.46). Following, at this stage,

the same steps as described in previous paragraph, we arrive first at

$$V_{\text{ring}}^{(i,j)} = \frac{m_i^3 T}{16\pi^{3/2}} \sum_{N=2}^{\infty} \sum_{r=1}^{N} \frac{(-1)^N (N-r)! (r-1)!}{N! \Gamma(N)}$$

$$V_{ring}^{(i,j)} = \frac{m_i^3 T}{16\pi^{3/2}} \sum_{N=2r=1}^{\infty} \frac{N}{N!} \frac{(-1)^N}{N!} \frac{(N-r)!(r-1)!}{\tilde{A}(N)} \times \Gamma(N-3/2) \Pi_{\mathbf{i}\Pi}^r \mathbf{j}^N - r_{\mathbf{i}}^2 \left(m_{\mathbf{i}}^2\right) - N$$
(III.58)

To perform the summation over N and r, we use the relation

$$\sum_{N=2}^{\infty} \sum_{r=1}^{N} f(N,r) = \sum_{N=2}^{\infty} f(N,N) + \sum_{r=1}^{\infty} \sum_{N=r+1}^{\infty} f(N,r)$$
 (III.59)

We thus obtain

$$V_{rin}^{(i,j}g) = V^{(i)} + V^{(i,j)}$$
(III.60)

with

$$V^{(i)} = \frac{m_{i}^{3}T}{16\pi^{3/2}} \sum_{N=2}^{\infty} \frac{(-1)^{N} \Gamma(N-3/2) \Pi_{i}^{N} \left(m_{i}^{2}\right)^{-N}}{\Gamma(N)}$$

$$V^{(i,j)} = \frac{m_{i}^{3}T}{16\pi^{3/2}} \sum_{r=1}^{\infty} \sum_{N=r+1}^{\infty} \frac{(-1)^{N} (N-r)!(r-1)!}{N!} \times \Gamma(N-3/2) \Pi_{i}^{N} \Pi_{i}^{j} \Gamma(m_{i}^{2})^{-N}$$
(III.61)

For V (i), the summation over N can be carried out and yields

$$V^{(i)} = \frac{T}{2L} \left[2 \left(m_i^2 + \Pi_i \right)^{3/2} - 2 m_i^3 - 3 m_i \Pi_i \right]$$
 (III.62)

As concerns $V^{(i,j)}$, we perform the summation over N and arrive at

$$V^{(i,j)} = \sum_{r=1}^{\infty} \frac{(-1)^{r+1}}{r} \frac{\Gamma(r-1/2)}{\Gamma(r+2)} \Pi_{i}^{r} \Pi_{j} \left(m_{i}^{2}\right)^{-r-1} \times_{3} F_{2} \left((1,2,r-1/2);(r+1,r+2);-\frac{\Pi_{j}}{m_{i}^{2}}\right), \quad \text{(III.63)}$$

where pFq(a;b;z) is the generalized hypergeometric function having the following series expansion

$${}_{\rho}F_{q}(\mathbf{a};\mathbf{b};z) = \sum_{k=0}^{\infty} \frac{(a_{1})_{k} \cdots (a_{\rho})_{k}}{(b_{1})_{k} \cdots (b_{\alpha})_{k}} \frac{z^{k}}{k!}$$
(III.64)

Here, $\mathbf{a} = (\mathbf{a}_1, \dots, \mathbf{ap}), \mathbf{b} = (\mathbf{b}_1, \dots, \mathbf{bq})$ are vectors with p and q components.

Moreover, $(a_1)k \equiv \Gamma(a_1+k)/\Gamma(a_i)$ is the Pochhammer symbol. For our purposes, it is suffi-cient to focus on the contribution at r = 1 in (III.63).

$$V^{(i,j)}\Big|_{r=1} = \frac{T}{24\pi} \left[2(m_i^2 + \Pi_j)^{3/2} - 2m_i^3 - 3m_i\Pi_j \right] \frac{\Pi_i}{\Pi_j} \quad \text{(III.65)}$$

Having in mind that the one-loop contribution to the self- energy Πi, which is determined in Sec. III B is of order $O(\lambda)$, the contributions corresponding to $r \ge 2$ are of order $O(\lambda 2)$ and can be neglected at this stage. We thus have

$$\begin{vmatrix}
C \\
V_{ring} &= V_{r}^{(2)} & (2) \\
g &= V^{(2)} + V^{(2,1)} \Big|_{r=1} \\
+O\left(\lambda^{2}, V_{ring}^{D} = V_{r}^{(in 1,2)} = V^{(1)} + V^{(1,2)} \right|_{r=1} + O\left(\lambda^{2}\right) \quad \text{(III.66)}$$

The final result for Vring is given by plugging Vr(I)ring, $I = A, \dots, D$ from (III.55) and (III.65) into (III.43),

$$\begin{split} &\mathcal{V}_{ring} = \frac{T}{24\pi} \left\{ \left(2 \left(m_{1}^{2} + \Pi_{2} \right)^{3/2} - 2m_{1}^{3} - 3m_{1}\Pi_{2} \right) \right. \\ &\left. + \left(2 \left(m_{2}^{2} + \Pi_{1} \right)^{3/2} - 2m_{2}^{3} - 3m_{2}\Pi_{1} \right) \right. \\ &\left. + \left(2 \left(m_{2}^{2} + \Pi_{2} \right)^{3/2} - 2m_{2}^{3} - 3m_{2}\Pi_{2} \right) \right. \\ &\left. + \left(2 \left(m_{1}^{2} + \Pi_{1} \right)^{3/2} - 2m_{1}^{3} - 3m_{1}\Pi_{1} \right) \right. \\ &\left. + \left(2 \left(m_{2}^{2} + \Pi_{1} \right)^{3/2} - 2m_{2}^{3} - 3m_{2}\Pi_{1} \right) \frac{\Pi_{2}}{\Pi_{1}} \right. \\ &\left. + \left(2 \left(m_{1}^{2} + \Pi_{2} \right)^{3/2} - 2m_{1}^{3} - 3m_{1}\Pi_{2} \right) \frac{\Pi_{1}}{\Pi_{2}} \right\} \\ &\left. + \mathcal{O} \left(\lambda^{2} \right) \right. \end{split}$$
(III.67)

Focusing only on the first perturbative correction to Πi and using $\Pi i(mat)i$, i = 1, 2 from (III.28), the above results is simplified as

$$V_{\text{ring}} \approx \frac{T}{8\pi} \sum_{i=1}^{2} \left[2(m_i^2 + \Pi^{\text{mat}})^{3/2} - 2m_i^3 - 3m_i \Pi^{\text{mat}} \right]$$
(III.68)

where
$$\Pi^{\text{mat}} = \Pi_1^{\text{mat}} = \Pi_2^{\text{mat}} = \frac{\lambda T^3 \zeta(3)}{2\pi^2 \Omega}$$
 (III.69)

F. Summary of Analytical Results in Sec. III

In this section, we summarize the main findings. According to these results, the total thermodynamic potential of a rigidly rotating Bose gas, Vtot, including the classical potential Vcl from (II.32) with c2 replaced with a2, the vacuum potential (II.33), the thermal part (II.34), 2and the ring potential (III.43) is given by

$$Vtot = V_{cl} + V_{vac} + V_{T} + Vring$$

$$\begin{split} & \text{V_{cl}} = -\frac{a^2 v^2}{2} + \frac{\lambda v^4}{4}, \\ & \text{V_{vac}} \approx -\frac{m_0^2 v^2}{4} + \frac{3c^2 \lambda v^2}{8\pi^2} + \frac{5m_0^2 \lambda v^2}{16\pi^2} - \frac{15\lambda^2 v^4}{64\pi^2} + \frac{m_0^2 \lambda v^4}{8a^2}, \\ & \text{V_{T}} \approx -\frac{2\,\text{T^5}\zeta(5)}{\pi^2 \Omega} + \frac{\lambda T^3 v^2 \zeta(3)}{\pi^2 \Omega} - \frac{c^2\,T^3 \zeta(3)}{2\pi^2 \Omega}, \\ & \text{V_{ring}} \approx + \frac{T}{8\pi} \Sigma_{i2}^2 \bigg(2 \bigg(m_i + \Pi^{\text{mat}} \bigg)_{3/2} - 2 m_i^3 - 3 m_i \Pi^{\text{mat}} \bigg) \end{split}$$

Here, $a^2 = c^2 + m_{Q_1}^2 m_{1}^2(v) = 3\lambda v^2 - c^2$ and $m_{2}^2(v) = \lambda v^2 - c^2$, and $\Pi^{mat} = \lambda T^3 \zeta(3) / 2\pi^2 \Omega$. We notice that the logarithmic terms appearing in Vvac from (III.42) are skipped in (III.70).

In the next section, we study the effect of rotation on the formation of condensate and the critical temperature of the global U(1) phase transition. To this purpose, we compare our results with the results arising from the full thermodynamic potential of a nonrotating Bose gas. ☑ According to [40], it is given by (Subscripts (0) correspond) to $\Omega = 0.$

$$V_{t}\begin{pmatrix}0\\\text{oot}\end{pmatrix} = V_{cl} + V_{vac} + V_{T}^{(0)} + V_{r}\begin{pmatrix}0\\in\end{pmatrix}g, \quad \text{(III.71)}$$

where V_{cl} and $V_{vac \, are \, given \, in \, (III.70), \, while} \, V_{T}^{\,\, (0)}$ and $V_{r}^{\,\, (0)} \, gread$

$$V_T^{(0)} \approx -\frac{\pi^2 T^4}{45} + \frac{\lambda T^2 v^2}{6} - \frac{c^2 T^2}{12},$$
 (III.72)

$$V_{r ing}^{(0)} \approx -\frac{7}{4\pi} \sum_{i_1} \left(2(m_i + \Pi_0)_{3/2} - 2m_i - 3m_i\Pi_0 \right) \text{ (III.73)}$$

one-loop self-energy $\Pi_0^{mat} = \lambda T^2 / 3[40]$ and m_i^2 , i = 1, 2 given as above.

IV. Numerical results

In this section, we explore the effect of rotation on different quantities related to the spontaneous breaking

of global U(1) symmetry. To this purpose, we consider different parts of Vtot from (III.69).

In Sec. III A, we derived the minimum of the potential

Va including Vcl and VT. We arrived at v_{min}^2 (T, Ω) from

(III.6). Replacing VT with $V_T^{(0)}$ from (III.72) for a nonrotating Bose gas and following the same steps leading from (III.4) to (III.6), we arrive at the critical temperature



$$T_c^{(0)} = \left(\frac{3a^2}{\lambda}\right)^{1/2} \tag{IV.1}$$

and the T dependent minima

$$v_{\min}^{2}(T) = \frac{\left\{a^{2}\right\}}{\lambda} (1 - t_{2}) \quad t_{n} < 1$$

$$(0, \quad t_{0} \ge 1)$$
(IV.2)

with the reduced temperature $t_0 = T/T_c^{(0)}$ and $T_c^{(0)}$ from (IV.1). In Figure 7, vm(2)min is plotted for $\Omega = 0$ [see (IV.2)] and $\Omega \neq 0$ [see (III.6)] as function of the corresponding reduced temperature t0 and t. The difference between these two plots arises mainly from different exponents of the corresponding reduced temperatures t0 and t in (IV.2) and (III.6). The reason of this difference lies in dif-ferent results for the high-temperature expansion of $T_c^{(0)}$ for $\Omega = 0$ [see (III.72)] and VT for $\Omega \neq 0$ [see (III.70)].

Let us consider Vtot - Vring = Vcl + V_{vac} + VT from (III.69). By minimizing this potential with respect to v, and solving the resulting gap equation,

$$\left. \frac{d}{d\overline{V}} \left(V_{\text{tot}} - V_{\text{ring}} \right) \right|_{\overline{V}_{\text{nin}}} = 0 \tag{IV.3}$$

it is possible to determine numerically the T dependence the minima, denoted by v-min (T,Ω) , for fixed Ω . To this purpose, we use the quantities a $\simeq 0.265$ GeV, c $\simeq 0.225$ GeV, and $\lambda =$ 0.5 given in (III.7). In Figure 8, the T/T $_{\circ}^{(0)}$ dependence of $ar{v}$ min is demonstrated for $\beta\Omega$ = 0.1, 0.2, 0.3 (dashed, dotted, and dotted-dashed curves). The results are then compared with the corresponding minima for a nonrotating Bose gas (red solid curve). The latter is determined by minimizing the combination $v_t(o_{ot}) - v_r(o_{in})$, according to

$$\frac{d}{dv}\left(V_{t o t}^{(0)} - V_{rinn}^{(0)}\right)^{T} \overline{v}_{min} = 0$$
 (IV.4)

with $V_t\binom{o}{ot}$ from (III.71). In both cases, $T_c^{~(0)} \approx o.681 \text{GeV}$ is the critical temperature of the spontaneous U(1) symmetry breaking in a nonrotating Bose gas. (The critical temperature is the temperature at which the condensate \bar{v} min vanishes.)

These results indicate that rotation lowers the critical temperature of the phase transition. However, as shown in Figure 8, Tc increases with increasing Ω . It is also im-portant to note that this same trend is observed in a noninteracting Bose gas under rigid rotation [30].

To answer the question whether the transition is continuous or discontinuous, we have to explore the shape of the potential, the value of its first and second order derivatives at temperatures below and above the critical

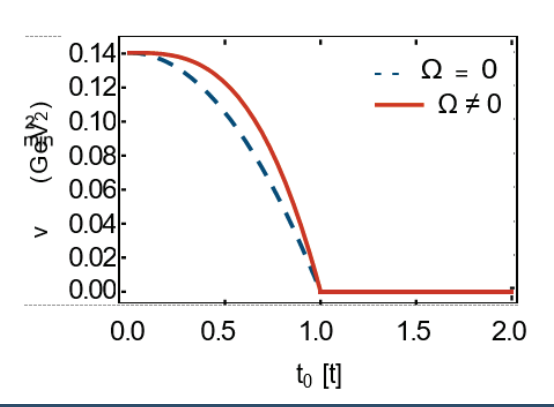


Figure 7: (color online). The t0 [t] dependence of v_{min}^2 (T) and v_{min}^2 (T, Ω) for nonrotating (Ω = 0) and rotating ($\Omega\neq 0$) Bose gas [see (III.6) and (IV.2)]. For Ω = 0 and $\Omega \neq 0$, the reduced temperature t0 or t is defined by t0 = T/T_c⁽⁰⁾ and t = T/T_d respectively.

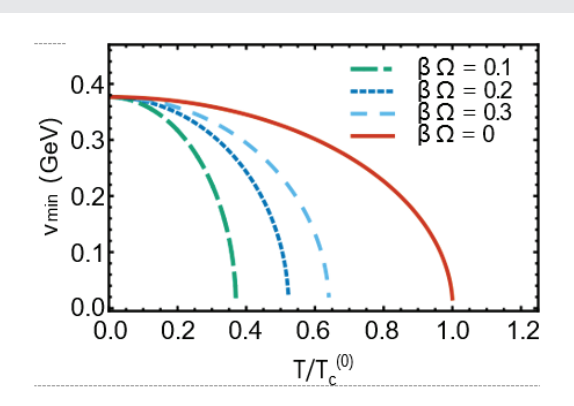


Figure 8: (color online). The $T/T_c^{(0)}$ dependence of \tilde{v} min is plot-ted for $\beta\Omega$ = 0, 0.1. 0.2, 0.3. For $\Omega \neq 0$ and $\Omega = 0$, v-min (T) arises by solving the gap equation (IV.3) and (IV.4), respectively. The temperature T is rescaled with $T_c^{(0)}$ = 0.681 GeV, the Ω independent critical temperature of a nonrotating Bose gas. It turns out that $Tc < T_c^{(0)}$ and for $\beta\Omega \neq 0$, Tc increases by increasing $\beta\Omega$.

temperature, Tc. Using the numerical values for the set of free parameters a, c, and λ as mentioned above, the transitions turns out to be continuous not only for $\Omega = 0$ but also for $\Omega \neq 0$.

To explore the effect of the ring potential on the temperature dependence of the condensate v-min, we solved numerically the gap equation

$$\frac{dV_{tot}}{dv}|_{\overline{V}_{min}} = 0$$
 (IV.5)

$$\frac{dV_t^{(\bar{\sigma})} Ot}{dv} \Big|_{\bar{v}_{\min}} = 0$$
 (IV.6)

for a rotating and a nonrotating Bose gas, respectively. The corresponding results are demonstrated in Figure 9. Because of the specific form of the ring potentials Vring and $V_{\rm r}^{\,(0)\,i}$ n from (III.70) and (III.73), including in particular $(m_i^2 + \Pi \text{mat})_3 / 2$, there is a certain value of v below which the

potential is undefined (imaginary). Let us denote this value by $\bar{v}\star$. In both rotating and non- rotating cases $v_{\perp} \simeq 0.319$ GeV. As it is shown in Figure 9, the minima decrease with increasing temperature and converge towards $\bar{v}\star$. Let us denote the temperature at which \bar{v}_{min} = v_{\star} with T* for Ω \neq 0 and $T_{\perp}^{(0)}$ for $\Omega = 0$. For $\Omega = 0$, $T_{\perp}^{(0)} \simeq 0.300$ GeV, and as it is shown in Figure 9, the transition to v* is discontinuous (red circles). For $\Omega \neq 0$, however, $T_{\star} < T_{\star}^{(0)}$ and increases with increasing $\beta\Omega$, similar to the results presented in Figure 8. Moreover, in contrast to the case of $\Omega = 0$, the transition to \bar{v}_{\perp} for all values of $\beta\Omega \neq 0$ is continuous.

In Figure 10, the phase diagram T_c - Ω is plotted for two cases: The blue solid curve demonstrates T_c from (III.5) arising from V_{cl} + VT. Red dots denote the Ω dependence of Tc arising from the potential Vtot - Vring. A comparison between these data reveals the effect of Vvac in increasing T_c . Apart from the Ω dependence of T_c , the Ω dependence of T* is demonstrated in Figure 10. It arises by adding the ring contribution to V_{cl} + VT + Vvac, as described above. According to the results demonstrated in Figure 10, considering Vring decreases Tc. But, simi- lar to $\mathrm{T_{c'}},\mathrm{T_{\star}}$ also increases with increasing Ω . It should be emphasized that the transition shown in Figure 8 is a crossover, since $\bar{v}_{\star} \neq 0$.

In Sec. III B, the masses m_i^2 , i = 1, 2 including the oneloop correction are determined [see (III.29)]. Identi- fying m_1^2 with m_{σ}^2 and m_2^2 with m_{π}^2 , we arrive at

$$m_{\pi}^{2}(v) = 3\lambda v^{2} - c^{2} + a^{2}t^{3},$$

 $m_{\pi}^{2}(v) = \lambda v^{2} - c^{2} + a^{2}t^{3}.$ (IV.7)

Using the data for $\overline{v}_{\it min}^{\it 2}$ arising from the solution of the gap equation (IV.3) and (IV.5), and evaluating $m_{\sigma}^{2}(v^{2})$ and $m_{\pi}^{2}(v^{2})$ from (IV.7) at \overline{v}_{min}^{2} for a fixed $\beta\Omega$, the $t = T/T_{c}$ dependence of m_1^2 and m_2^2 is determined. In Figure 11(a), the dependence of $m_\sigma^2\big(\overline{\nu}_{\min}^2\big)$ and m $^2\big(\overline{\nu}_{min}^2\big)$ with vmin arising from (IV.3) on the reduced tempera- ture t = T / Tcis plotted for fixed $\beta\Omega = 0.1$. Here, the contribution of the ring potential is not taken into ac-count. Hence, a continuous phase transition occurs with the critical temperature Tc ~ 0.399GeV for $\Omega = 0.1$ GeV. In contrast, in Figure 11(b), m_{σ}^2 and m_{π}^2 are determined by plugging the data of \bar{V} min arising from (IV.5), with Vtotincluding the ring potential. Hence, the difference between the plots demonstrated in Figs. 11(a) and 11(b) arises from the contribution of the nonperturbative ring potential. As we have mentioned above, when the ring potential is taken into account, the data demonstrated in Figure 9 do not describe a true transition, since $\overline{\nu}_{\star}$ is not zero. The reduced temperature

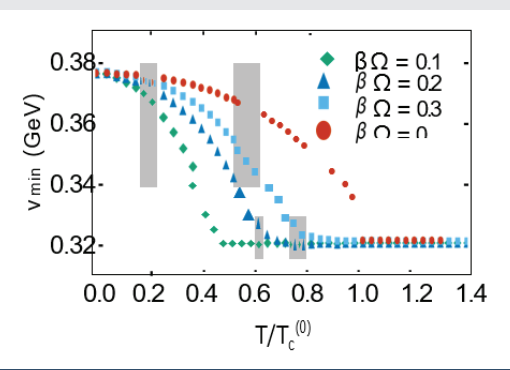


Figure 9: (color online). The T/T_c⁽⁰⁾ dependence of \tilde{v} min is plot-ted for $\beta\Omega$ = 0, 0.1, 0.2, 0.3. For $\Omega \neq 0$ and $\Omega = 0$, v-min (T) arises by solving the gap equation (IV.5) and (IV.6), respec- tively. Here, \tilde{v}_{\star} = 0.319 GeV and $T_{\star}^{(0)}$ = 0.300 GeV. It turns out that T_{\star} < $T_{\star}^{(0)}$ and for $\beta\Omega \neq 0$, T_{\star} increases by increasing $\beta\Omega$.

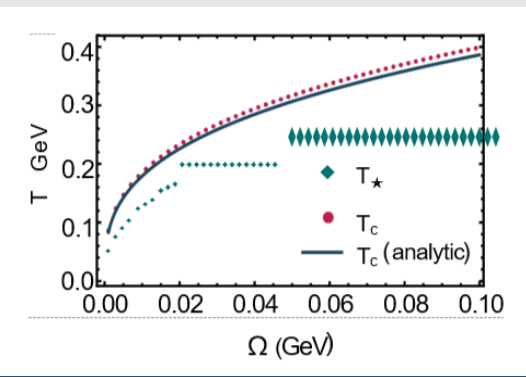


Figure 10: (color online). The Ω dependence of the transition temperatures is plotted. The blue solid line is the transition temperature T $_{c~\alpha}$ $\Omega^{1/3}$ from (III.5). It arises from V_{al} + VT, as described in Sec. III A. Red dots correspond to the critical temperatures Tc, arising from Vtot - Vring. Green diamonds denote T, arising from Vtot

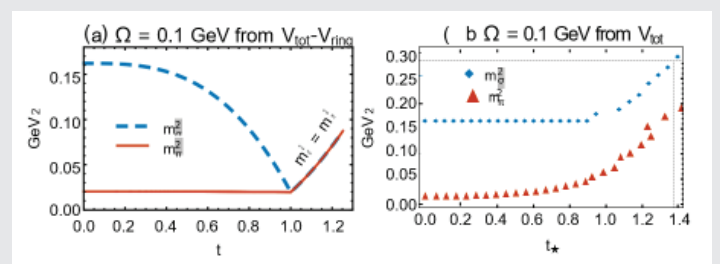


Figure 11: (color online). (Panel a) The t = T/Tc dependence of $m_{\sigma}^2(v-min)$ and $m_{\pi}^2(v-min)$ from (IV.7) is plotted for $\Omega = 0.1$ GeV. The data of \tilde{V}_{min} arise by solving the gap equation (IV.3) corresponding to Vtot – Vring. The critical temperature Tc for Ω = 0.1 GeV is Tc \sim 0.399 GeV. As expected from the case of nonrotating Bose gas, in the symmetry-restored phase at $t \ge 1$, $m_{\sigma}^2 = m_{\tau}^2$. (Panel b) The t* dependence of $m_{\sigma}^2(v^*)$ and $m_{\tau}^2(v^*)$ from (IV.7) is plotted for $\Omega = 0.1$ GeV. The data of \tilde{v} min arise by solving the gap equation (IV.5). corresponding to Vtot which includes the nonperturbative ring potential. According to Figure 10, for $\Omega = 0.1$ GeV, we have $T^* \sim 0.278$ GeV. At $t \ge 1$, $m_{\pi}^2 - m_{\pi}^2 = 2\lambda \tilde{V}^*(2)^*$, with $\tilde{v}_* \simeq 0.319$ GeV from Figure 9 and $\lambda = 0.5.$

in Figure 11(b) is thus defined by $t_{\downarrow} = T/T_{\downarrow}$, where, according to the data pre-sented in Figure 10 T_{\perp} ~ 0.278GeV for Ω = 0.1.

Let us compare the results demonstrated in Figure 11(a) with that in Figure 5. In both cases, before the phase transition at $t < 1, m_{\sigma}^2$ decreases with increasing t. Moreover, whereas in Figure 5, M_{π}^2 remains constant, it slightly decreases once the Vvac contribution is taken into account.

After the transition, at $t < 1, m_{\sigma}^2$ becomes equal to M_{π}^2 and they both increase with increasing t. It is straight- forward to verify this statement using equation (IV.7). Given that, in this case, the minima of the potential at $t \ge 1$ are zero, it follows that both masses are equal, specifically $m_{\sigma}^{2}(0) = m_{\pi}^{2}(0)$, once we substitute \overline{v} min = 0 into (IV.7).

in the framework of fermionic Nambu-Jona-Lasinio (NJL) model: As noted in [45], in the symmetry-broken phase, $m_{\sigma}^2 > m^2$. As the transition temperature is approached, m_{σ}^2 decreases, and at a certain dissociation temperature Tdiss, the masses m_{σ} and m_{π} become de-generate. This temperature is characterized by m_{σ} (Tdiss) 2 = m_{π} (Tdiss). (IV.8)

This behavior is expected from the case of $\Omega = 0$ and

As it is described in [45], σ mesons dissociates into two pions because of the appearance of an s-channel pole in the scattering amplitude $\pi + \pi \rightarrow \pi + \pi$. In this process a σ meson is coupled to two pions via a quark triangle. In the symmetry-restored phase, at $t \geq 1, m_{\sigma}$ becomes equal to $m\pi$. They both increase with increasing T [45,46].

In Table 1, the σ dissociation temperatures are listed for $\Omega = 0,0.1,0.2,0.3$ GeV. The data in the second (third) column correspond to Tdiss $(T_d^* iss)$ for the case when $\overline{V}_{\text{min}}$ is the solution of (IV.3) [(IV.5)] for $\Omega \neq 0$ and (IV.4) [(IV.6)] for $\Omega = \mathbf{0}$. Comparing Thiss and $\mathsf{T}_{\mathsf{d}}^{\star}$ is with T_{C} and T_{\perp} shows that T diss < Tc and similarly $T_{diss}^{\star} < T_{\star}$ The property T diss \neq Tc is because we are working with $m\pi \neq 0$. Let us notice that, as aforementioned, the σ dissociation temperature is originally introduced in a fermionic NJL model [45]. In this model, nonvanishing $m\pi$ indicates a nonvanishing quark bare mass mo, and choosing $\tilde{m}_{0} \neq 0$ implies a crossover transition characterized by Tdiss \neq Tc. It seems that in the bosonic model studied in the present work, a nonvanishing pion mass leads similarly to T diss \neq Tc.

The behavior demonstrated in Figure 11 (a) changes once the contribution of the ring potential is taken into account As it is shown in Figure 11 (b) in the symmetry broken phase

Table 1: 0.2, 0.3 GeV is compared with the critical temperature Tc and crossover temperature T*. In the second column, the data arise from the solution of the gap equation (IV.3) and (IV.4). In the third column, the data arise from the solution of the gap equation (IV.5) and (IV.6). In both cases the dissociation temperature is lower than the transition temperatures.

| Ω in GeV | Tdiss [Tc] in GeV | Td(*)diss [T*] in GeV |
|----------|-------------------|-----------------------|
| 0 | 0.584 [0.681] | 0.220 [0.300] |
| 0.1 | 0.322 [0.399] | 0.210 [0.278] |
| 0.2 | 0.418 [0.502] | 0.271 [0.358] |
| 0.3 | 0.480 [0.576] | 0.316 [0.416] |

at $t_{\star} < 1, m_{\sigma}$ decreases slightly with T while $m\pi$ increases with T Moreover in contrast to the case in which Vring is not taken into account m_{π} and $m\pi$ are not equal at $t \ge 1$ This observation highlights the ef fect of nonperturbative ring contributions on the relation between m_{π} and $m\pi$ mainly in the symmetry restored phase. This behavior is directly related to the fact that the effect illustrated in Figure 9 is a crossover once the ring contribution is considered. Plugging \mathbf{u}_{-} into (IV.7) the masses of σ and π mesons are given by

$$\begin{array}{l} m_{\sigma}^{2}(u_{\star}) = 3\lambda u_{\star}^{2} - c^{2} + a^{2}t^{3} \\ m_{\pi}^{2}(u - \star) = \lambda u_{\star}^{2} - c^{2} + a^{2}t^{3} \end{array} \tag{IV.9}$$

Their difference is thus given by $m_\sigma^2(u-\star)-m_\pi^2(u-\star)=2\lambda u_-^2$ and remains constant in t This fact can be observed in Figure 11 (b) at $t_{\downarrow} \geq 1$.

V. Summary and conclusions

In this paper, we extended the study of the effects of rigid rotation on BE condensation of a free Bose gas in [30], to a self-interacting charged Bose gas under rigid rotation. In the first part, we considered the Lagrangian density of a complex scalar field \mathcal{G} with mass m, in the presence of chemical potential μ and angular velocity Ω . The interaction was introduced through a $\lambda(\mathcal{D}\star\mathcal{D})$ term. This Lagrangian is invariant under global U(1) transfor- mation. To investigate the spontaneous breaking of this symmetry, we chose a fixed minimum with a real component u, and evaluated the original Lagrangian around this minimum to derive a classical potential. Then, we applied an appropriate Bessel-Fourier transformation to determine the free propagator of this model, expressed in terms of two masses m1 and m2, corresponding to the two components of the complex field. These masses depend explicitly on $u_i\lambda_i$, and m_i and played a crucial role when the spontaneous breaking of U(1) symmetry was consid- ered in a realistic model that includes σ and π mesons. Using the free boson propagator of this model, we derived the thermodynamic potential of selfinteracting Bose gas at finite temperature T. This potential consists of a vac- uum and a thermal part. Along with the classical poten-tial, this forms the total thermodynamic potential of this model Vtot from (II.24). This potential is

expressed in terms of the energy dispersion relation $\in_{\mathbf{k}}^{\pm}$ from (II.15), and explicitly depends on $l\Omega$. A novel result presented here is that, although $l\Omega$ appears to resemble

a chemical potential in combination with $\in_{\mathbf{k}}^{\pm}$ in Vtot, the

effec-tive chemical potential μ eff = μ + $l\Omega$ appears solely in a noninteracting Bose gas under rotation (see the special case 1 in Sec. II D and compare the thermodynamic potential with that appearing in [30]).

For $\lambda, \mu \neq 0$, we explored two cases $\mu > m$ and $\mu < m$. The former corresponds to the phase where U(1) symme-try is broken, while the latter describes the symmetry-restored phase. By expanding the two branches of the energy dispersion relation around $k \sim 0$ in the symmetry-broken

phase, we identified $\in_{\mathbf{k}}^{\pm}$ and $\in_{\mathbf{k}}^{-}$ as phonon and roton, with the latter representing a massless Goldstone mode. Upon comparison with analogous results for a nonrotating and self-interacting Bose gas, we found that rigid rotation

does not alter the behavior of $\in^{\pm}_{\mathbf{k}}$ at $k \sim 0$. This is mainly because rotation appears in terms of $l\Omega$ within Vtot, rather than directly affecting $\in_{\mathbf{k}}^{\pm}$.

In the second part of this paper, we examined the effect of rigid rotation on the spontaneous breaking of U(1) symmetry in an interacting Bose gas at $\mu = 0$ (see Sec. III). In this case, where $m^2 < 0$, we replaced m^2 with $-c^2$, where $c^2 > 0$. By introducing an additional term to the original Lagrangian, we defined a new mass, $a^2 = c^2 +$ m_0^2 . We demonstrated that the minimum of the classical potential is nonzero, indicating a sponta- neous breaking of U(1) symmetry. We then addressed the question about the position of this minimum, specif- ically its dependence on T and Ω , after accounting for the thermal part of the effective potential combined with the classical potential. To investigate this, we performed a high-temperature expansion of the thermal part of the potential, utilizing a method originally introduced in [30]. This approach enabled us to sum over the angular mo- mentum quantum numbers ℓ for small values of $\beta\Omega$, allowing us to derive both the critical temperature of the phase transition Tc and the dependencies of the mini- mum of the potential on T and Ω . At this stage, we have $T_c \propto \lambda^{-1/3}$, which is in contrast to the $T_c^{(0)} \propto \lambda^{-1/2}$ for a nonrotating Bose gas. In addition, T_c $\propto \Omega$ $^{1/3}.$ Let us remind that the critical temperature of a BEC transi- tion for a noninteracting Bose gas in nonrelativistic and ultrarelativistic limits are T $_{_{\rm C}} \propto \Omega^{2/5}$ and T $_{_{\rm C}} \propto \Omega^{1/4}$, respectively [30]. This demonstrates the effect of rotation in changing the critical exponents of different quantities in the symmetry-broken phase.

We defined a reduced temperature t = T/Tc, and showed that in the symmetry-broken phase, the minimum mentioned above depends on $(1-t^3)$, while for a nonrotating Bose gas this dependence is $(1-t_0^2)$, where $t_0 = T/T_c^{(0)}$. In the symmetry-restored phase, this minimum vanishes. This indicates a continuous phase transition in both nonrotating and rotating Bose gases. Plugging these minima into $m_1^2(v)$ and $m_2^2(v)$, it turned out that at $t \ge 1$, i.e., in the symmetry-restored phase m^1 and m^2 are imaginary. Since, according to our arguments in Sec. III, m^2 is the mass of a Goldstone mode, we expect that in the chiral limit, i.e., when $m_0 = 0$, it vanishes in the symmetry- broken phase at t < 1. However, as it is shown in (III.13), $m_2^2 < 0$ in this phase.

To resolve this issue, we followed the method used in [40] and added the thermal part of one-loop self-energy diagram to the above results. In contrast to the case of nonrotating bosons, where the thermal mass square is proportional to λT^2 , for rotating bosons it is proportional to $\lambda T^3/\Omega$. To arrive at this result, a summation over ℓ was necessary. This was performed by utilizing a method originally introduced in [30]. Adding this perturbative contribution to m_i^2 , i = 1, 2 at t < 1 and $t \ge 1$, we showed that the Goldstone theorem is satisfied in the chiral limit [see Sec. III Cl.

In Secs. III D and III E, we added the vacuum and nonperturbative ring potentials to the classical and thermal potentials. The main novelty of these sections lies in the final results for these two parts of the total potential, specifically the method we employed to sum over ℓ . According to this method the vacuum part of the potential for a rigidly rotating Bose gas is the same as that for a nonrotating gas. We followed the method described in [43] to dimensionally regularize the vacuum potential. As concerns the ring potential, we present a novel method to compute this nonperturbative contribution to the thermodynamic potential. In particular, we summed over ℓ by performing a ζ-function regularization. In Sec. III F, we presented a summary of these results.

In Sec. IV, we used the total thermodynamic poten-tial presented in Sec. III to study the effect of rotation on the spontaneous U(1) symmetry breaking of a realistic model including σ and π mesons. Fixing free parameters m_{σ} , m_{π} , and λ , and identifying m_1 and m_2 with the meson masses $m\sigma$ and $m\pi$, we obtained numerical values for c and a (see Sec. III A). First, we determined the T de-pendence of the minima of the total thermodynamic po- tential, excluding the ring contribution. According to the results presented in Figure 8, rotation decreases the critical temperature of the U(1) phase transition. Additionally, it is shown that Tc increases with increasing Ω . In [30], it is shown that the critical temperature of the BEC in a noninteracting Bose gas under rotation behaves in the same manner. This phenomenon indicates that rotation enhances the condensation. Recently, a similar result was observed in [47], where it is demonstrated that the inter- play between rotation and magnetic fields significantly increases the critical temperature of the superconducting phase transition.

To explore the effect of nonperturbative ring potential, we numerically solved the gap equation corresponding to the total thermodynamic potential and determined its minima \bar{v} min. Because of the specific form of the ring potential, there was a certain $\bar{v}\star$ through which all the curves v-min (T, Ω f), independent of the chosen Ω f, converge (see Figure 9). Moreover, the transition for $\Omega=0$ turned out to be discontinuous, while it is continuous for all $\Omega \neq 0$. As it is demonstrated in Figure (10), T \star increases with increasing Ω .

Finally, we determined the *T* dependence of the masses m_a and m_a mesons for a fixed value of Ω . To achieve this, we utilized (IV.7) along with \bar{v} min, which is derived from Figs. 8and 9. The plot shown in Figure 11(a), based on the total potential excluding the ring contribu-tion, is representative of the T dependence of m σ and m π (see e.g., [46]). However, when we include the ring contribution, the shape of the plots changes, especially at T > T*. The reason is that considering the ring potential changes the order of the phase transition from a second order transition to continuous (for $\Omega \neq 0$) or discontinuous (for $\Omega = 0$) a crossover. In this context, we numer- ically determined the σ dissociation temperature Tdiss, which may serve as an indicator for type of the transi-tion into the symmetryrestored phase. We showed that Tdiss < T₂ and Tdiss < T⋆, as expected from a crossover transition [46].

It would be intriguing to extend the above findings, in particular those from Sec. III, to the case of nonvanish- ing chemical potential. In [48], the kaon condensation in a certain color-flavor locked phase (CFL) of quark mat- ter is studied at nonzero temperature. This is a state of matter which is believed to exist in quark matter at large densities and low temperatures. Large densities at which the color superconducting CFL phase is built are expected to exist in the interior of neutron stars. One of the main characteristic of these compact stars, apart from densities, is their large angular velocities. It is not clear how a rigid rotation, like that used in the present paper, may affect the formation of pseudo-Goldstone bosons and the critical temperature of the BE condensation in this nontrivial environment. We postpone the study of this problem to our future publication.

Acknowledgment

We thank the University of Tokyo's Department of Science for theoretical support and resources.

(Appendix)

References

- Yagi K, Hatsuda T, Miake Y. Quark-gluon plasma: From big bang to little bang. Cambridge: Cambridge University Press; 2005; 446.
 Available from: https://inspirehep.net/literature/702469
- Fukushima K, Hatsuda T. The phase diagram of dense QCD. Rep Prog Phys. 2011;74:014001.
 Available from: https://doi.org/10.1088/0034-4885/74/1/014001
- Busza W, Rajagopal K, van der Schee W. Heavy ion collisions: The big picture, and the big questions. Annu Rev Nucl Part Sci. 2018;68:339.
 Available from: https://arxiv.org/abs/1802.04801

- Bzdak A, Esumi S, Koch V, Liao J, Stephanov M, Xu N. Mapping the phases of quantum chromodynamics with beam energy scan. Phys Rept. 2020;853:1.
 Available from: https://inspirehep.net/literature/1737718
- Aarts G, Aichelin J, Allton C, Athenodorou A, Bachtis D, Bonanno C, et al. Phase transitions in particle physics: Results and perspectives from lattice quantum chromodynamics. Prog Part Nucl Phys. 2023;133:104070. Available from: https://arxiv.org/abs/2301.04382
- Boyanovsky D, de Vega HJ, Schwarz DJ. Phase transitions in the early and the present universe. Annu Rev Nucl Part Sci. 2006;56:441.
 Available from: https://arxiv.org/abs/hep-ph/0602002
- Laine M, Vuorinen A. Basics of thermal field theory. Lect Notes Phys. 2016;925:1.
 - Available from: https://arxiv.org/abs/1701.01554
- Skokov V, Illarionov AY, Toneev V. Estimate of the magnetic field strength in heavy-ion collisions. Int J Mod Phys A. 2009;24:5925.
 Available from: https://arxiv.org/abs/0907.1396
- Shen D, Chen J, Huang XG, Ma YG, Tang A, Wang G. A review of intense electromagnetic fields in heavy-ion collisions: Theoretical predictions and experimental results. Research. 2025;8:0726.
 Available from: https://spj.science.org/doi/10.34133/research.0726
- Fayazbakhsh S, Sadooghi N. Phase diagram of hot magnetized two-flavor color superconducting quark matter. Phys Rev D. 2011;83:025026.
 Available from: https://journals.aps.org/prd/abstract/10.1103/ PhysRevD.83.025026
- Fayazbakhsh S, Sadeghian S, Sadooghi N. Properties of neutral mesons in a hot and magnetized quark matter. Phys Rev D. 2012;86:085042.
 Available from: https://journals.aps.org/prd/abstract/10.1103/ PhysRevD.86.085042
- Fukushima K. Extreme matter in electromagnetic fields and rotation. Prog Part Nucl Phys. 2019;107:167.
 Available from: https://arxiv.org/abs/1812.08886
- Becattini F, Karpenko I, Lisa M, Upsal I, Voloshin S. Global hyperon polarization at local thermodynamic equilibrium with vorticity, magnetic field and feed-down. Phys Rev C. 2017;95:054902.
 Available from: https://journals.aps.org/prc/abstract/10.1103/ PhysRevC.95.054902
- Becattini F, Lisa MA. Polarization and vorticity in the quark-gluon plasma. Annu Rev Nucl Part Sci. 2020;70:395-423.
 Available from: https://www.annualreviews.org/content/journals/10.1146/annurev-nucl-021920-095245
- Yamamoto A, Hirono Y. Lattice QCD in rotating frames. Phys Rev Lett. 2013;111:081601.
 Available from: https://arxiv.org/abs/1303.6292
- Available from: https://arxiv.org/abs/1303.6292
- Chernodub MN, Gongyo S. Interacting fermions in rotation: Chiral symmetry restoration, moment of inertia and thermodynamics. JHEP. 2017;01:136.
 Available from: https://arxiv.org/abs/1611.02598
- Chernodub MN, Gongyo S. Effects of rotation and boundaries on chiral symmetry breaking of relativistic fermions. Phys Rev D. 2017;95:096006.
 Available from: https://journals.aps.org/prd/abstract/10.1103/ PhysRevD.95.096006
- Ambruş VE, Winstanley E. Exact solutions in quantum field theory under rotation. 2019.

 Available from: https://orgiv.org/obs/1008.10244
 - Available from: https://arxiv.org/abs/1908.10244
- Sadooghi N, Tabatabaee Mehr SMA, Taghinavaz F. Inverse magnetorotational catalysis and the phase diagram of a rotating hot and magnetized quark matter. Phys Rev D. 2021;104:116022.
 Available from: https://journals.aps.org/prd/abstract/10.1103/ PhysRevD.104.116022



- 20. Sun F, Shao J, Wen R, Xu K, Huang M. Chiral phase transition and spin alignment of vector mesons in the polarized-Polyakov-loop Nambu-Jona-Lasinio model under rotation. Phys Rev D. 2024;109:116017. Available from: https://journals.aps.org/prd/abstract/10.1103/ PhysRevD.109.116017
- 21. Kharzeev DE, Liao J, Voloshin SA, Wang G. Chiral magnetic and vortical effects in high-energy nuclear collisions: a status report. Prog Part Nucl Phys. 2016:88:1-28.

Available from: https://doi.org/10.1016/j.ppnp.2016.01.001

22. Mameda K, Yamamoto A. Magnetism and rotation in relativistic field theory. PTFP 2016:2016:093B05 Available from: https://academic.oup.com/ptep/

article/2016/9/093B05/2468923

- 23. Chen HL, Fukushima K, Huang XG, Mameda K. Analogy between rotation and density for Dirac fermions in a magnetic field. Phys Rev D. 2016;93:104052. Available from: https://journals.aps.org/prd/abstract/10.1103/ PhysRevD.93.104052
- 24. Chernodub MN. Inhomogeneous confining-deconfining phases in rotating plasmas. Phys Rev D. 2021;103:054027. Available from: https://journals.aps.org/prd/abstract/10.1103/ PhysRevD.103.054027
- 25. Braguta VV, Chernodub MN, Roenko AA, Sychev DA. Negative moment of inertia and rotational instability of gluon plasma. Phys Lett B. 2024:852:138604 Available from: https://doi.org/10.1016/j.physletb.2024.138604
- 26. Braguta VV, Chernodub MN, Kudrov IE, Roenko AA, Sychev DA. Negative Barnett effect, negative moment of inertia of the gluon plasma, and thermal evaporation of the chromomagnetic condensate. Phys Rev D. 2024;110:014511.

Available from: https://journals.aps.org/prd/abstract/10.1103/ PhysRevD.110.014511

- 27. Ambruş VE, Chernodub MN. Rigidly rotating scalar fields: Between real divergence and imaginary fractalization. Phys Rev D. 2023;108:085016. Available from: https://journals.aps.org/prd/abstract/10.1103/ PhysRevD.108.085016
- 28. Siri E, Sadooghi N. Thermodynamic properties of a relativistic Bose gas under rigid rotation. Phys Rev D. 2024;110:036016. Available from: https://journals.aps.org/prd/abstract/10.1103/ PhysRevD.110.036016
- 29. Siri E, Sadooghi N. Boson propagator under rigid rotation. Trans Theor Math Phys. 2024;1:105. Available from: https://www.arxiv.org/abs/2408.06194
- 30. Siri E, Sadooghi N. Bose-Einstein condensation in a rigidly rotating relativistic boson gas. Phys Rev D. 2025;111:036011. Available from: https://journals.aps.org/prd/abstract/10.1103/ PhysRevD.111.036011
- 31. Kuboniwa R, Mameda K. Finite-temperature perturbation theory of rotating scalar fields. 2025. Available from: https://arxiv.org/abs/2504.04712
- 32. Voskresensky DN. Charged pion vortices in rotating systems. Phys Part Nucl Lett. 2024;21:1036. Available from: https://inspirehep.net/literature/2781242
- 33. Voskresensky DN. Pion condensation at rotation in magnetic field, electric, and scalar potential wells. Phys Rev D. 2025;111:036022. Available from: https://journals.aps.org/prd/abstract/10.1103/ PhysRevD.111.036022

34. Bordag M, Pirozhenko IG. Casimir effect for scalar field rotating on a disk. EPL. 2025;150:52001.

Available from: https://arxiv.org/abs/2505.14093

35. Bordag M, Voskresensky DN. Generation of a scalar vortex in a rotational frame. 2025.

Available from: https://journals.aps.org/prd/abstract/10.1103/y2lc-27pn

36. Singha P, Ambruş VE, Chernodub MN. Inhibition of the splitting of the chiral and deconfinement transition due to rotation in QCD: The phase diagram of the linear sigma model coupled to Polyakov loops. Phys Rev D. 2024:110:094053

Available from: https://arxiv.org/abs/2407.07828

- 37. Hernández LA, Zamora R. Vortical effects and the critical end point in the linear sigma model coupled to quark. Phys Rev D. 2025;111:036003. Available from: https://journals.aps.org/prd/abstract/10.1103/ PhysRevD.111.036003
- 38. Morales-Tejera S, Ambruş VE, Chernodub MN. Firewall boundaries and mixed phases of rotating quark matter in linear sigma model. 2025. Available from: https://journals.aps.org/prd/abstract/10.1103/4zrn-wgrg
- 39. Singha P, Busuioc S, Ambruş VE, Chernodub MN. Linear sigma model with quarks and Polyakov loop in rotation: Phase diagrams, Tolman-Ehrenfest law and mechanical properties. Phys Rev D. 2025;112:094031. Available from: https://journals.aps.org/prd/abstract/10.1103/knn8-sv3k
- 40. Kapusta JI, Gale C. Finite-temperature field theory: Principles and applications. 2nd ed. Cambridge: Cambridge University Press; 2007. Available from: https://library.oapen.org/bitstream/ handle/20.500.12657/64016/9781009401968.pdf?sequence=1&isAllowed=y
- 41. Schmitt A. Dense matter in compact stars: A pedagogical introduction. Lect Notes Phys. 2010:811:1. Available from: https://arxiv.org/abs/1001.3294
- 42. Schmitt A. Introduction to superfluidity: Field-theoretical approach and applications. Lect Notes Phys. 2015;888:1. Available from: http://ndl.ethernet.edu.et/bitstream/123456789/73852/1/72. pdf.pdf
- 43. Carrington ME. The effective potential at finite temperature in the standard model. Phys Rev D. 1992;45:2933. Available from: https://journals.aps.org/prd/abstract/10.1103/ PhysRevD.45.2933
- 44. Anchishkin D, Gnatovskyy V, Zhuravel D, Mishustin I, Stoecker H. Four types of phase transitions in interacting boson (meson) matter at high temperatures. J Subatomic Part Cosmol. 2025;4:100073. Available from: https://arxiv.org/abs/2506.21736
- 45. Quack E, Zhuang P, Kalinovsky Y, Klevansky SP, Hufner J. π – π scattering lengths at finite temperature. Phys Lett B. 1995;348:1. Available from: https://arxiv.org/abs/hep-ph/9410243
- 46. Buballa M, Heckmann K, Wambach J. Chiral restoration effects on the shear viscosity of a pion gas. Prog Part Nucl Phys. 2012;67:348. (No URL provided.)
- 47. Chernodub M, Wilczek F. Enhanced condensation through rotation. 2025;1. Available from: https://arxiv.org/abs/2501.01734
- 48. Alford MG, Braby M, Schmitt A. Critical temperature for kaon condensation in color-flavor locked quark matter. J Phys G. 2008;35:025002. Available from: https://arxiv.org/abs/0707.2389